NCAR/TN-396+STR
NCAR TECHNICAL NOTE

December 1993

Vertical Interpolation and Truncation of Model-Coordinate Data

Kevin E. Trenberth
Jeffery C. Berry
Lawrence E. Buja

CLIMATE AND GLOBAL DYNAMICS DIVISION

NATIONAL CENTER FOR ATMOSPHERIC RESEARCH
BOULDER, COLORADO

Table of Contents

Preface

This technical note explores the advantages and disadvantages of using global analyses on 1) pressure level surfaces, and 2) model (sigma or hybrid) level surfaces and the issues of interpolation from one to the other, time averaging, changing resolution, and extrapolation below ground. Documentation is provided of the new algorithms implemented in the Community Climate Model (CCM) modular processor for deriving pressure-level data from model-level (hybrid or sigma) data.

Model levels consist, in simplest form, of a sigma (σ) terrain-following coordinate in which the lowest level corresponds to $p = p_s$, where p is pressure and p_s is the surface pressure and $\sigma = p/p_s$. Hybrid levels consist of sigma near the surface but with a gradual transition to pressure with height (often above about 100 mb). One major issue with data on such levels is that the model surface often does not correspond with the earth's real surface. Another is that a change in horizontal resolution is not well defined because the vertical coordinate also changes in the process. For instance, a reduction from high resolution with 106 waves (T106 resolution) to a moderate resolution with 42 waves (T42), so as to reduce the size of datasets by a factor of about 6, is often desirable. A third issue involves the meaning and use of time averages on model surfaces and their relationship to corresponding time averages on pressure surfaces. The traditional representation on constant pressure surfaces has much to recommend it and is widely used and familiar to the community, but suffers from errors arising from interpolation to the pressure surfaces and the need to properly treat regions of those surfaces that are below ground (in regions of high topography).

Algorithms used to go from model to pressure levels in the CCM have been quite simple in the past and produce very unrealistic-looking features near mountains where below-ground influences are important. In addition, they differ from algorithms used by the major operational centers, the National Meteorological Center (NMC) and the European Centre for Medium Range Weather Forecasts (ECMWF), thereby leading to some difficulties when trying to validate the CCM. Accordingly, the ECMWF algorithms for interpolating to pressure surfaces and extrapolating below ground have been implemented in the CCM processor, and an additional new algorithm is documented for sea level pressure. Those algorithms and their effects are documented here.

This implementation permits comprehensive testing of the problems in changing

resolution. Because spectral truncation and resolution changes are well defined on pressure surfaces, test results are presented for cases where T106 analyses on model surfaces are 1) transformed to pressure and then truncated, 2) truncated and then transformed to pressure levels, and 3) then compared at comparable resolutions. The differences arise mainly from the ill-posed truncation on model surfaces, but also from vertical interpolations. These tests are also applied to a heat budget calculation involving nonlinear terms for one month. However, the latter comparison also brings in considerations of how best to do time averaging and the fact that a time average on model surfaces is inherently different than a time average on pressure surfaces. Fortunately, in practical terms, the differences are quite small and probably negligible for most purposes.

The magnitude of the various errors from vertical interpolation and truncation, and the degree to which they project on scales of interest is documented. The acceptability of these errors will depend on the application. The results show that truncation on model surfaces from T106 to T42 produces errors considerably larger than vertical interpolation errors. However, truncation to T63 for computations produces more acceptable truncation errors provided that only T31 waves are retained as reasonably accurate.

Acknowledgments

This research was partially supported by the Tropical Oceans Global Atmosphere (TOGA) Project Office under grant NA87AANRG0208 and by NASA under "NCAR Project to Interface Climate Modeling on Global and Regional Scales with Earth Observing System (EOS) Observations," NASA Order No. W-18,077. The data were supplied by ECMWF and NMC. Jim Hurrell provided useful comments.

Cover

The cover illustration shows the ECMWF surface pressure at T42 resolution. The truncation is performed for $\ln p_s$ and a taper has been applied. This constitutes p for the lowest model coordinate level.

Special Note, second printing, May 1994

In this second printing, some small corrections were made to Figs. 21 to 29 along with minor changes in the text.

1. Introduction

Global analyses of various quantities are needed to carry out comprehensive diagnostic studies. The most convenient global data sets for this purpose are the global analyses produced operationally for weather forecasting purposes (Fortelius and Holopainen 1990, Trenberth 1991a). These are produced using a four-dimensional data assimilation system in which multivariate observed data are combined with the "first guess" using a statistically optimum scheme. The first guess is the best estimate of the current state of the atmosphere from previous analyses produced using a numerical weather prediction (NWP) model.

The global analyses are produced on model (sigma or hybrid) surfaces; at the U.S. National Meteorological Center (NMC) these are sigma surfaces and at the European Centre for Medium Range Weather Forecasts (ECMWF) they are hybrid surfaces (Fig. 1). In both cases the surfaces are defined relative to the surface pressure field on the lowest model level which follows the topography of the surface of the earth, as represented in the model. The hybrid scheme is essentially a sigma coordinate at low levels and a pressure coordinate above about 100 mb. Analyzed variables are interpolated or extrapolated onto constant pressure surfaces in the postprocessing stages using various schemes.

The nature of the interpolation scheme and whether it preserves physical relationships among variables is a critical issue which has been explored to some extent by Shen et al. (1986) and Trenberth (1991a). For the ECMWF analyses, Trenberth (1991a) shows that mass is not conserved by the analyses on pressure surfaces evidently because of the methods of postprocessing the data. It appears that the interpolation procedure used by ECMWF produces the most accurate values possible at the archived levels, but they are not representative values for finite sized layers. While it would be possible to ensure that a constraint such as conservation of mass is achieved, for instance by recomputing omega using the kinematic method (O'Brien 1970), it is clear that a loss of accuracy would occur and there is no reason why the interpolated divergence rather than omega field should be preferred. Consequently, there are several sources of error in the equation of continuity in pressure coordinates. From Trenberth (1991a), these include:

$P_{k+\frac{1}{2}} = A_{k+\frac{1}{2}} + B_{k+\frac{1}{2}} Ps$,

$A_{k+\frac{1}{2}}$ (hPa)	$B_{k+\frac{1}{2}}$
10	0
20	0
40	0
60	0
83	0.004
106	0.014
128	0.035
146	0.072
158	0.127
161	0.202
153	0.296
136	0.405
111	0.524
82	0.645
52	0.759
26	0.856
8	0.929
0	0.973
0	0.992
0	1

Vertical Coordinate Table (NL=19)

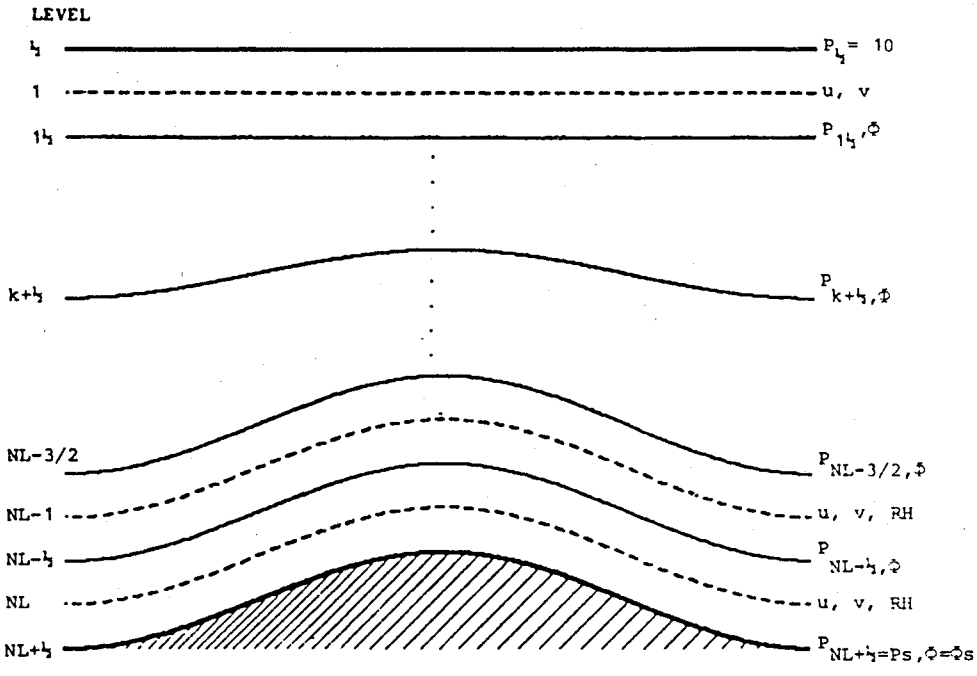

Disposition of variables in the vertical

Domain	Global	
Data assimilation frequency	6-hr (± 3-hr observation time window)	
First guess	6-hr forecast	
Dependent variables	Ps, Φ, u, v, RH	
Vertical coordinate	Hybrid, $P_{k+\frac{1}{2}} = A_{k+\frac{1}{2}} + B_{K+\frac{1}{2}} Ps$, details as above	
Horizontal grid	160 x 320 points on a quasi-regular (1.125°) "Gaussian" grid	
Analysis method	Mass and wind:	3-dimensional multi-variate statistical interpolation
	Relative humidity:	3-dimensional uni-variate statistical interpolation up to 250 hPa
	Surface:	Sea surface temperature from NMC analysis
		Soil water content using rainfall observations, estimated evaporation
		Snow depth using snow depth and snowfall observations
Initialisation method	Non-linear normal mode, 5 vertical modes, non-adiabatic	

Fig. 1. The ECMWF analysis system in 1987. Shown are the levels, the A and B values (also Table 1) and some brief descriptive aspects of the analysis system.

1) errors arising from the vertical interpolation and the fact that archived values are really level values and not necessarily representative of layers; and

2) the vertical resolution of the resulting archive.

In addition, further work has revealed that there are substantial problems in the vicinity of the surface of the earth and extrapolation below ground. In part these arise from the fact that the earth's surface in the analyses and the real world differ, and in part they arise from the desire to use constant pressure surfaces for variables, so that the earth's topography above mean sea level or 1000 mb is replaced by an artificial atmosphere everywhere.

At ECMWF an enhanced "envelope orography" is used, which places the earth's surface at surface pressures up to 100 mb or more lower in value (Trenberth 1992). At NMC a "silhouette orography" was used until 6 March 1991, when it was replaced by "mean mountains". Justification of the enhanced topographic heights is made on the grounds that the free atmosphere does not dynamically connect with air in valleys. In both cases the representation is spectral, so that the surface has extensive ripples over the ocean, arising from Gibbs phenomena.

In validating model output, such as from the NCAR Community Climate Model CCM2, it has been necessary to carry out similar forms of postprocessing from the model (in this case hybrid) coordinates to pressure levels for comparison with the climatologies based on the analyses from the operational archives (e.g., Trenberth and Olson 1988, Trenberth 1992). In the past, the methods of postprocessing in the CCM modular processor, in particular extrapolation below ground, have differed from those at the operational centers, and indeed the procedures at the two operational centers also differ. Consequently, differences and apparent errors can arise solely from these differences in postprocessing.

Also, because of the interpolation errors noted above, it seems desirable in working quantitatively with the global analyses that diagnostic calculations should be performed on model rather than pressure surfaces (e.g., Hoerling and Sanford 1993). However, other difficulties related to the resolution of the data set then arise and the problem of model validation still exists because the differing model surfaces are not the same. The resolution question raised here refers to horizontal resolution and it becomes important because the

model coordinate systems will vary depending on the scales resolved. This is true even if the same vertical coordinate and levels are used. The problem is equivalent to one of changing the resolution from, say T106, to T42 resolution on model coordinates. At the high T106 resolution, detailed topographical features can be captured that are not present in the lower T42 resolution model and the result is that the surface pressures and thus the model coordinates will contain more structure. This problem is considerably exacerbated by the use of enhanced artificial lower boundary surfaces (envelope orography at ECMWF or silhouette orography at NMC). Unfortunately, it is not a trivial problem to change resolution on model coordinates because the model coordinate itself changes so that horizontal and vertical gradients of variables become confounded.

Yet a further problem exists in working on model surfaces, and that is the process and meaning of time averaging. As a time average is performed, the surface pressure and thus the model coordinate itself also becomes time averaged. Thus the definition of a time-averaged quantity in model coordinates and its relationship to the corresponding time average in pressure coordinates is not at all clear. Any interpolation of the model-coordinate time average to pressure using the time-averaged pressure clearly ignores a contribution from the covariance between the surface pressure and the variable in question. In practice this difference is usually assumed small, but this assumption needs to be tested. In any event, such a time average cannot then be mass weighted to produce vertical integrals. Instead, it seems that it should be the layer mass-weighted variable that should be time averaged.

Consequently, in this note we explore these three problems of interpolation from model to pressure coordinates, appropriate methods for truncating model coordinate data, and ways of time averaging. Horizontal smoothing on pressure surfaces is well posed and methods for truncating spherical harmonics at lower resolution are described in Trenberth and Solomon (1993) and Trenberth (1992). Similar truncation is not well posed with sigma surfaces. To change resolution on sigma surfaces, it appears to be necessary to first interpolate to pressure, then truncate, and finally interpolate back to sigma. Ironically, the main advantage of working in model coordinates to avoid vertical interpolation errors is immediately lost. These aspects are explored further below.

2. Data sets

The main global analyses used for illustration here are from the ECMWF although completely parallel analyses and algorithms exist for the NMC analyses. The issues are of importance in all global atmospheric data sets. In this study we have used an archive of the ECMWF analyses on model hybrid coordinates as well as the ECMWF WCRP analyses on pressure p coordinates at 14 levels in the vertical four-times daily (Trenberth 1992). The 14 levels available from the ECMWF WCRP archive are p = 1000, 850, 700, 500, 400, 300, 250, 200, 150, 100, 70, 50, 30 and 10 mb. The latter are uninitialized analyses whereas the model-level data are initialized, so the comparison of the model data interpolated to p with the pressure-level data is not clean. The hybrid level scheme at ECMWF is described by Simmons and Burridge (1981) and Simmons and Strüfing (1983).

For NMC we have used sigma-level data and the corresponding p data for the same times from separate archives to test the algorithms.

3. Vertical interpolation and extrapolation

3.1 ECMWF Vertical interpolation and extrapolation

Given $NL = 19$ full levels in the model (Fig. 1), with level $k = 1$ at the top and $k = 19$ at the bottom, the disposition of variables in the analyses at ECMWF is such that u, v, and RH are defined as the full model levels while geopotential Φ or geopotential height z is defined on the half levels. In the model, the p values corresponding to the model half levels are given by

$$p_{k+\frac{1}{2}} = A_{k+\frac{1}{2}} + B_{k+\frac{1}{2}} p_s \qquad (1)$$
$$k = 1, ...NL$$

where the $A_{k+\frac{1}{2}}$ and $B_{k+\frac{1}{2}}$ are given in Table 1. As noted by Simmons and Strüfing (1983), the full-level pressures are given by the Eq. (3.18) of Simmons and Burridge (1981). We have taken this expression for many values of p_s and used linear regression to determine the corresponding A_k and B_k values for the same formulation as in (1). In all cases, exceptionally good fits were found with correlations for p_s ranging from 600 to 1020 hPa of 1.0000, a standard error of 0.0 for B_k and less then 0.006 hPa for A_k at all levels (i.e., in the sixth decimal place). Values of the A_k and B_k are also given in Table 1.

From Table 1 it can be seen that the hybrid system becomes purely pressure above 70 mb and is purely sigma below $\sigma = 0.973$. The surface elevation $z_s = \Phi_s/g$ at T63 resolution is shown in Fig. 2.

Several previous algorithms for vertical interpolation and extrapolation in the CCM have existed although the primary ones that have been used are simple linear in σ or linear in $ln(\sigma)$, with the latter the default. This is equivalent to linear in lnp. In the free atmosphere the latter works well for most quantities. At ECMWF interpolations for geopotential height are performed in $\ln\eta$, while η is used for other variables, where η is the hybrid vertical coordinate. (This point is somewhat unclear as several options are discussed in the ECMWF documentation, including interpolation using splines under tension. But a personal communication with ECMWF indicates that the splines are not used in practice, in spite of the documentation (ECWMF 1990)).

The following notes are based on Appendix 6 (Post processing) of the ECMWF Re-

Table 1. Values of A_k, B_k, $A_{k+\frac{1}{2}}$ and $B_{k+\frac{1}{2}}$ for $NL = 19$ levels for the ECMWF model in 1987. A_k is in hPa. Also shown is the pressure level if $p_s = 1000$ hPa.

k	A_k	B_k	p for $p_s = 1000$ hPa
$\frac{1}{2}$	10	0	10
1	15	0	15
$1\frac{1}{2}$	20	0	20
2	29.4	0	29.4
$2\frac{1}{2}$	40	0	40
3	49.7	0	49.7
$3\frac{1}{2}$	60	0	60
4	71.2	.0019	71.4
$4\frac{1}{2}$	83	0.004	87
5	94.3	.0088	103.1
$5\frac{1}{2}$	106	0.014	120
6	116.9	.0241	141.0
$6\frac{1}{2}$	128	0.035	163
7	137.0	.0528	189.8
$7\frac{1}{2}$	146	0.072	218
8	152.1	.0986	250.7
$8\frac{1}{2}$	158	0.127	285
9	159.8	.1635	323.3
$9\frac{1}{2}$	161	0.202	363
10	157.4	.2479	405.3
$10\frac{1}{2}$	153	0.296	449
11	144.9	.3494	494.3
$11\frac{1}{2}$	136	0.405	541
12	123.9	.4635	587.4
$12\frac{1}{2}$	111	0.524	635
13	96.8	.5836	680.4
$13\frac{1}{2}$	82	0.645	727
14	67.3	.7014	768.7
$14\frac{1}{2}$	52	0.759	811
15	39.2	.8071	846.3
$15\frac{1}{2}$	26	0.856	882
16	17.1	.8923	909.4
$16\frac{1}{2}$	8	0.929	937
17	4.1	.9509	954.9
$17\frac{1}{2}$	0	0.973	973
18	0	.9825	982.5
$18\frac{1}{2}$	0	0.992	992
19	0	.9960	996.0
$19\frac{1}{2}$	0	1.0	1000

search Manual 2 as available in 1990, see also Haseler and Sakellarides (1986). For sea level pressure additional procedures are described.

a. Geopotential on model half levels

$$\Phi_{NL+\frac{1}{2}} = \Phi_s \tag{2}$$

$$\Phi_{k-\frac{1}{2}} = \Phi_{k+\frac{1}{2}} + R_d T_{vk} \ell n \left(\frac{p_{k+\frac{1}{2}}}{p_{k-\frac{1}{2}}} \right) \qquad 1 \leq k \leq NL \tag{3}$$

$$\Phi_{\frac{1}{2}} = \Phi_{1\frac{1}{2}} + R_d T_{v1} 2\ell n 2 \tag{4}$$

where T_{vk} is the virtual temperature on level k.

b. Mean sea level pressure.

Mean sea level pressure is computed from the surface pressure plus an assumption of a dry hydrostatic subterranean atmosphere with a uniform lapse rate of 6.5×10^{-3} Km^{-1} but modified slightly for exceptionally warm or cold conditions. If the height of the surface is less then 10^{-4}m then $p_{msl} = p_s$.

A surface temperature T_* is computed

$$T_* = T_{NL} + .0065 \frac{R_d}{g} T_{NL} \left(\frac{p_s}{p_{NL}} - 1 \right) \tag{5}$$

Define

$$\alpha = .0065 \frac{R_d}{g} \tag{6}$$

then a constant lapse rate of .0065 Km^{-1} gives

$$T = T_* + \frac{\alpha}{R_d}(\Phi_s - \Phi). \tag{7}$$

The hydrostatic equation is

$$\frac{\partial \Phi}{\partial p} = \frac{-R_d T}{p} \tag{8}$$

from which we obtain

$$T = T_* (\frac{p}{p_s})^{\alpha} \tag{9}$$

$$\Phi = \Phi_s - \frac{R_d T_*}{\alpha} \left((\frac{p}{p_s})^{\alpha} - 1 \right) \tag{10}$$

$$p_{msl} = p_s \left(1 + \frac{\alpha \Phi_s}{R_d T_*} \right)^{(1/\alpha)} \tag{11}$$

For small α (11) is approximated as

$$p_{msl} = p_s \exp\left[\frac{\Phi_s}{R_d T_*}\left(1 - \frac{1}{2}\left(\frac{\alpha\Phi_s}{R_d T_*}\right) + \frac{1}{3}\left(\frac{\alpha\Phi_s}{R_d T_*}\right)^2\right)\right] \tag{12}$$

However, for very high or low temperatures, α is modified as follows.

If $T_* \leq 290.5$K and $T_o > 290.5$K, where

$$T_o = T_* + .0065\Phi_s/g \tag{13}$$

α is reduced to

$$\alpha = \frac{R_d}{\Phi_s}(290.5 - T_*) \tag{14.1}$$

If $T_* > 290.5$K and $T_o > 290.5$K then $\alpha = 0$ and

$$T_* \text{ is set to } \frac{1}{2}(290.5 + T_*) \tag{14.2}$$

If $T_* < 255$K then

$$T_* \text{ is set to } \frac{1}{2}(255 + T_*) \tag{14.3}$$

(14.1) and (14.2) inhibit low pressures under hot elevated terrain and (14.3) inhibits unduly high pressures below elevated cold terrain.

The above procedure seems to work reasonably well as long as the surface height is less than about 2000 m elevation. Problems remain especially in the Himalayan-Tibetan Plateau region. At very high elevations, the critical dependence on the local surface temperature that is used to set the temperature of the whole artificial below-ground column becomes amplified and leads to considerable noise in the mean sea level pressure. The surface and near-surface temperature varies with time of day and surface topography, for instance, when cold air is trapped in valleys. Observing practices account for the diurnal cycle by recommending use of the average of the current temperature and that of twelve hours earlier. This is typically not done by operational centers or modeling groups.

In order to increase the representativeness of the virtual temperature applied to the below ground column, Mesinger and Treadon (1993) have suggested a technique for horizontal extrapolation of virtual temperatures observed in the free atmosphere around the mountainous area. This then is intended to replace what is essentially a vertical extrapolation of temperature using a standard lapse rate. They designed a rather involved procedure that performs a two dimensional interpolation which requires solution at each level of a

Laplace equation with the temperatures at the sides of the mountain serving as boundary conditions, beginning from the top of the mountain and progressing down. In testing the performance of the procedure in the NMC eta model, they find a great benefit of substantial reduction in noise in the resulting product over operational NMC procedures, which are similar to those outlined above.

We have chosen a simpler application of this principle for elevations above 2000 m. The steps are as follows:

1. Compute the mean sea level pressure everywhere using the above ECMWF techniques.
2. Given the mountain height at a grid point, p_t the pressure at mountain top height at neighboring points can be computed from the geopotential heights as a function of pressure outside the mountain. Thus the difference $\Delta p = p_{msl} - p_t$ can be estimated for the points both east and west of the mountain point where the elevation does not exceed 2000 m. This procedure takes advantage of the known p_{msl} and gives Δp as the effective column virtual temperature outside the mountain.
3. Interpolate Δp for all regions below ground where the elevation exceeds 2000 m except in Antarctica. The interpolation is performed only in the east-west direction. To ensure that there is no undue influence of the mountain itself and to make the procedure robust to changes in resolution, we choose the first points to the east and to the west where the surface elevation is less than 1250 m. To avoid any discontinuities, the interpolation is then carried out for all interior points, i.e. all points for which the mountain height exceeds 1250 m. (Note, however, this step is triggered only if the mountain exceeds 2000 m in elevation).
4. Add the interpolated Δp to p_s at the mountain point to get the new p_{msl}.

The implementation first identifies for each latitude, the string of points which qualify for recalculation. For each model and resolution, this need be done only once. The 2000 m and 1250 m critical values that are involved in the extra adjustment are ad hoc and perhaps could be tuned to produce better results. We have not pursued that aspect. The regions affected and the difference between the 1250 and 2000 m elevation contours can be seen in Fig. 2.

The method takes advantage of the fact that an estimate of p_{msl} already exists and thus the column integrated virtual temperature contribution can be obtained by a simple pressure difference. The value of p_t will require an interpolation in the vertical to the mountain point height using the analyzed geopotential at the model levels, and this interpolation should be linear in z and ln p. Note that the column-integrated virtual temperature used will be a combination of that computed for the free atmosphere above the surrounding points plus the extrapolated temperature below ground. The latter can be for a layer up to 1250 m thick and needs to be included to ensure that no spatial discontinuities are introduced.

The simplification introduced here over the Mesinger method is to do the interpolation in only one direction, east-west, and only for elevations above 1250 m in the neighborhood of peaks over 2000 m height. Depending on resolution, this may require interpolations in Greenland, the Mexican highlands and the Rockies throughout North America, in the Himalayan-Tibetan plateau region, and for the Andes. In addition, there are a few isolated spots in Africa, Europe, New Zealand, New Guinea and some other parts of Asia. Clearly, an east-west interpolation does not work for Antarctica, but is straightforward elsewhere. Over Antarctica, the ECMWF procedures seem to work quite well anyway; consequently, the added procedure is not implemented south of 60°S.

It is not clear what criterion should be used to judge the success or otherwise of the mean sea level pressure reduction. One technique would be to compare with observations which use a different algorithm, but one that is also flawed. Instead, we believe that the goal should be to remove the signature of the mountain itself from the field, although distortion of isobars through orographic effects must be allowed for.

c. Geopotential below ground

Below ground geopotential is treated as for mean sea level pressure. Eq. (10) is approximated (cf. also (16) given below)

$$\Phi = \Phi_s - R_d T_* \ell n \frac{p}{p_s} \left[1 + \frac{1}{2} \alpha \ell n \frac{p}{p_s} + \frac{1}{6} \left(\alpha \ell n \frac{p}{p_s} \right)^2 \right] \tag{15}$$

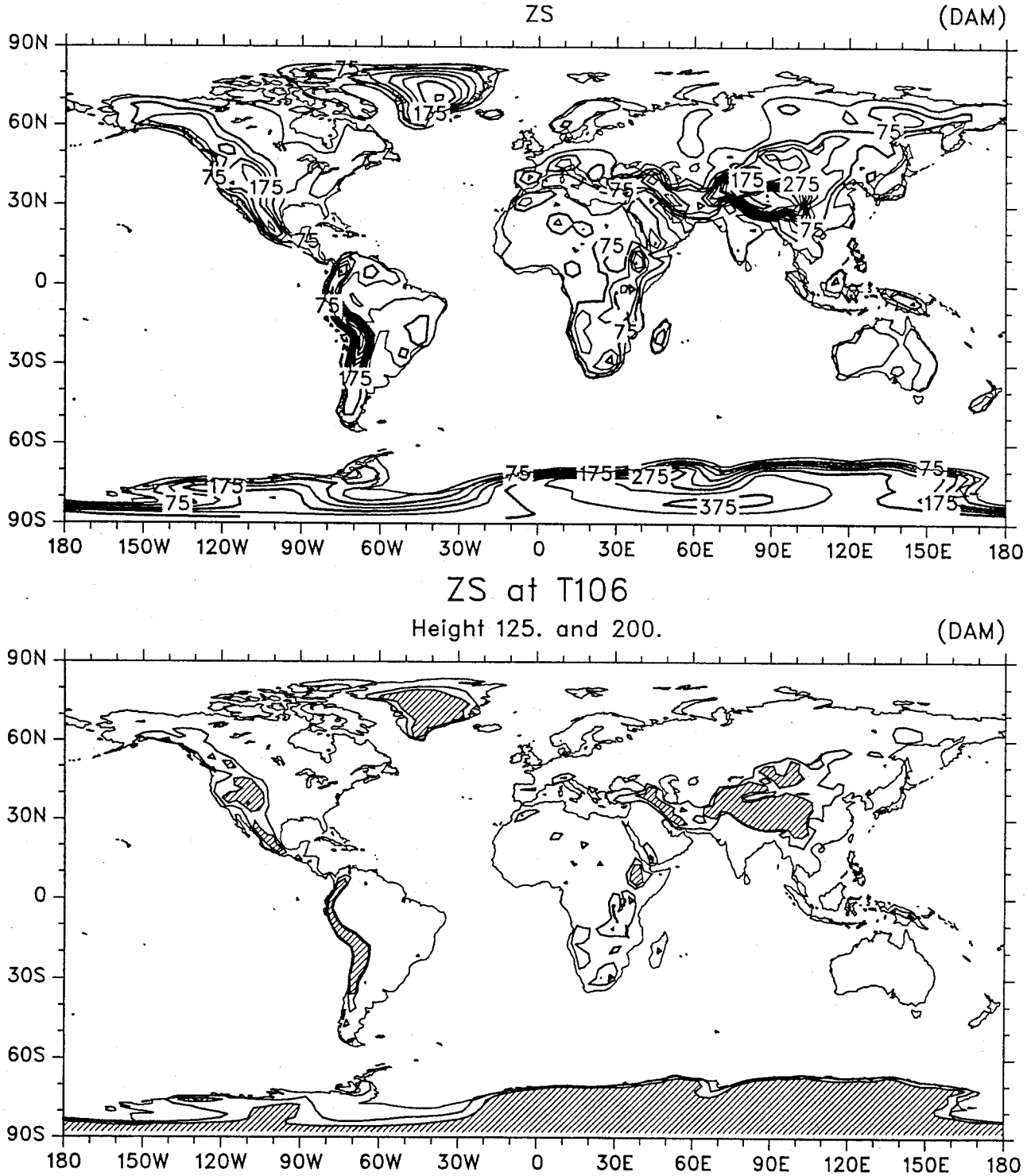

Fig. 2. Surface height field at T63 resolution (with highest wavenumbers tapered) for the ECMWF analysis in which envelope (enhanced) orography is included (top). Units are dam and the contour interval is 500 m, with a reference contour of 25 dam. Contours of the 2000 m and 1250 m elevation are shown in the bottom panel at T106 resolution, with regions higher than 2000 m stippled. Excepting Antarctica, these are the regions for which the additional procedure is implemented for computing sea level pressure.

d. Temperature below ground

To extrapolate temperature below ground, (9) is approximated as

$$T = T_* \left(1 + \alpha \ell n \frac{p}{p_s} + \frac{1}{2}(\alpha \ell n \frac{p}{p_s})^2 + \frac{1}{6}(\alpha \ell n \frac{p}{p_s})^3\right) \tag{16}$$

with T_* defined as in (5) and $\alpha = .0065 \frac{R_d}{g}$ for $\frac{\Phi_s}{g} < 2000$ m. For high orography, this is modified with

$$\alpha = R_d(T_o' - T_*)/\Phi_s \tag{17}$$

where, defining

$$T_{p\ell} = \text{Min}(T_o, 298) \tag{18}$$

$$T_o' = T_{p\ell} \text{ for } \Phi_s/g > 2500\text{m} \tag{19a}$$

or

$$T_o' = .002\left[(2500 - \Phi_s/g)T_o + (\Phi_s/g - 2000)T_{p\ell}\right] \tag{19b}$$

for $2000 \leq \Phi_s/g \leq 2500$ m. and T_o is given by (13). If $T_o' < T_*, \alpha$ is set to zero.

e. Other variables

For u, v, ω and RH, values are simply held constant below ground at the values from the lowest model level.

3.2 Results

In the free atmosphere, the vertical interpolation is unchanged.

Figure 3 shows results of using the former procedures for below-ground extrapolations on the NMC analyses for the temperature at 700 mb. Here the top panel shows for one day (1 September 1991) the archived pressure field from NMC, the middle panel shows the interpolated/extrapolated field using the CCM processor from the NMC sigma data archive, and the lower panel shows the differences. Huge discrepancies are apparent over Antarctica and the Himalayan plateau region, showing the inadvisability of simply linearly extrapolating below ground rather than using the procedures outlined earlier.

With the revised algorithms given above, Fig. 4 shows the corresponding interpolated NMC field and the difference from the NMC-archived field. Because we have implemented the ECMWF procedures for extrapolation below ground, which differ from the NMC proce-

dures, differences are expected, but they are nevertheless much less than in Fig. 3 and the field is not charcterized by "bullseyes". Figure 4 then provides a measure of the discrepancies that can still be expected from differing procedures.

Results for the 1000 mb geopotential height field z are given in Figs. 5 and 6. Fig. 5 shows the NMC 1000 mb analysis for 1 September 1991 at 0000 UTC along with the result from the original extrapolation procedures in the processor. Problems are immediately apparent over the Himalayas and Greenland where differences exceed 12 dam over Greenland and are as high as 28 dam in the Himalayas. Over Antarctica, the two fields are similar but the gradients are more exaggerated in the old CCM processor procedures and differences are as large as 20 dam. An alternative version of the truth is the corresponding ECMWF analysis for the same time, given in the top panel of Fig. 6. Very large differences exceeding 30 dam exist between the ECMWF and NMC analyses and are due primarily to the algorithms for extrapolating below ground. Thus application of the ECMWF algorithm to the NMC analyses and the difference with the NMC 1000 mb analysis (Fig. 6) shows a similar pattern. Differences are as large as 33 dam over Antarctica, but the analysis there is continuous and reasonable and does not follow the orography (as it tends to do in the NMC analysis), and the bullseyes over Greenland and the Himalayan complex are eliminated.

For sea level pressure, the tests made were much more demanding because it is so widely used. As well as testing at T42 resolution, we also tested extensively at T106 resolution, and it was this that led us to pursue the new procedures on top of the ECMWF algorithms, see section 3.1.b.

Fig. 7 shows the p_{msl} for 1 January 1991 from original analyses on model hybrid coordinates from ECMWF (i) as produced using the former default algorithm from the CCM Processor, and (ii) as produced using the ECMWF algorithm alone. The contour interval is 5 mb to show up the problem areas. In the latter, the extremely high values over Antarctica and Greenland are ameliorated, but the analysis is degraded over the Andes where an additional closed high pressure contour is introduced. Both methods produce exceptionally noisy plots over the Tibetan Plateau. Figure 8 shows the same field with the full new algorithm implemented as well as the difference from that using the ECMWF procedure alone. Notable differences occur over the Andes, the Tibetan Plateau, Greenland, and the central

Rockies. Moreover, in every case, the aesthetic look of the analysis is substantially improved. In the Tibetan Plateau region, the new analysis is not without remaining noise, but it is more benign and does not stand out. The noise is no longer present with a small amount of smoothing or lower resolution.

The new algorithm was also tested for situations with the seasons reversed, and Figs. 9 and 10 show equivalent maps for 1 July 1990. Of note is that the new procedure has produced an adjustment about as large in the Tibetan Plateau region (exceeding 15 mb) but of opposite sign. The improvement in the appearance of the analyses is every bit as impressive as for January, with no sign of the Andes or Greenland in the new analysis at all, unlike the other versions. We consider this a very desirable characteristic.

Clearly, application of the new algorithm in the CCM processor will facilitate comparisons of model results with ECMWF analyses. Discrepancies with NMC analyses will remain, but the fields are generally much more realistic and acceptable than with the previous procedure.

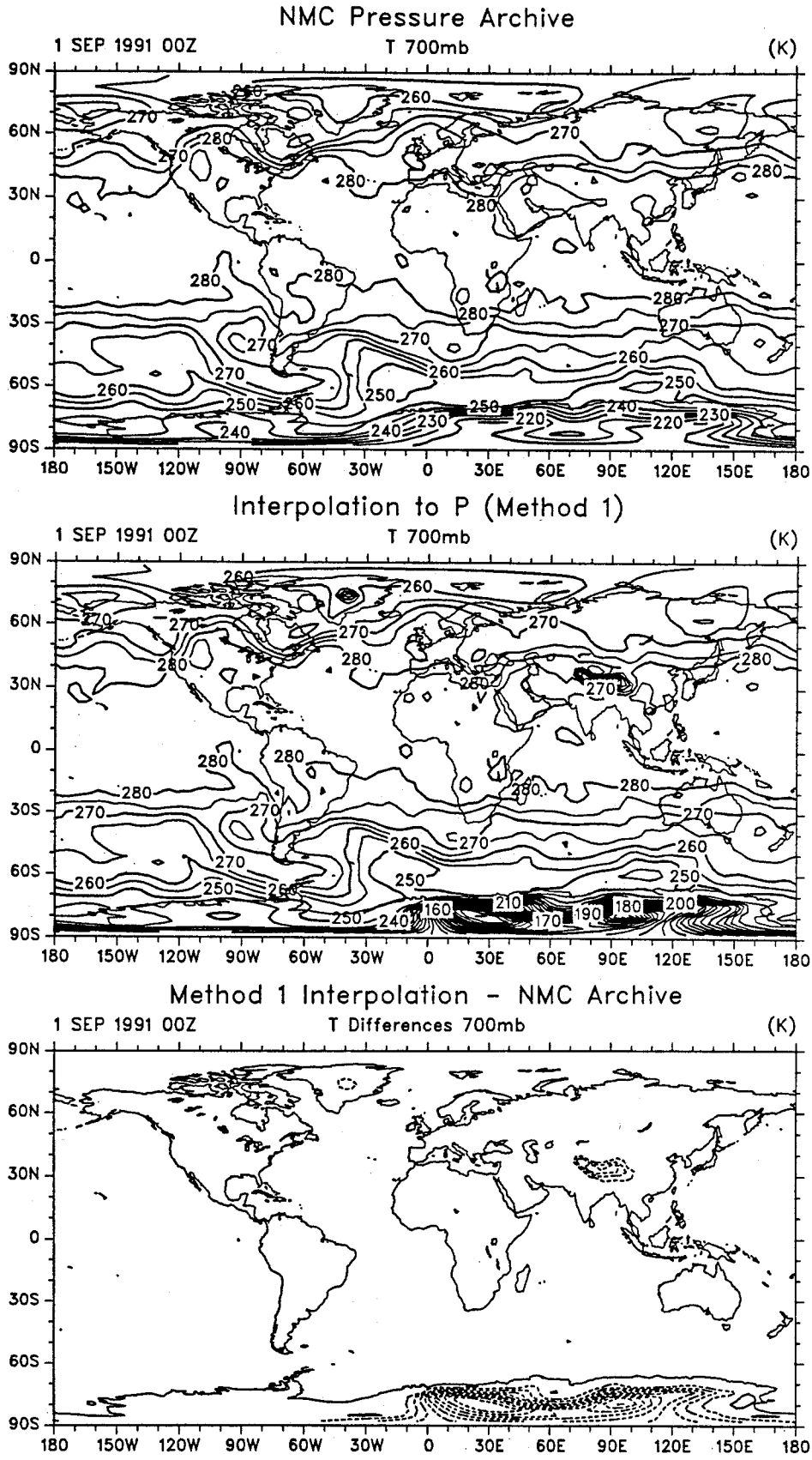

Fig. 3. For 1 September 1991 at 0000 UTC, shown are the temperature analysis from NMC at 700 mb, as obtained from the NMC archive (top), the corresponding field interpolated using former CCM procedures from NMC analyses on σ surfaces (middle) and their differences (bottom). The contour interval is 5° C in the top two panels and 10° C in the bottom. The zero contour is omitted and negative values are dashed.

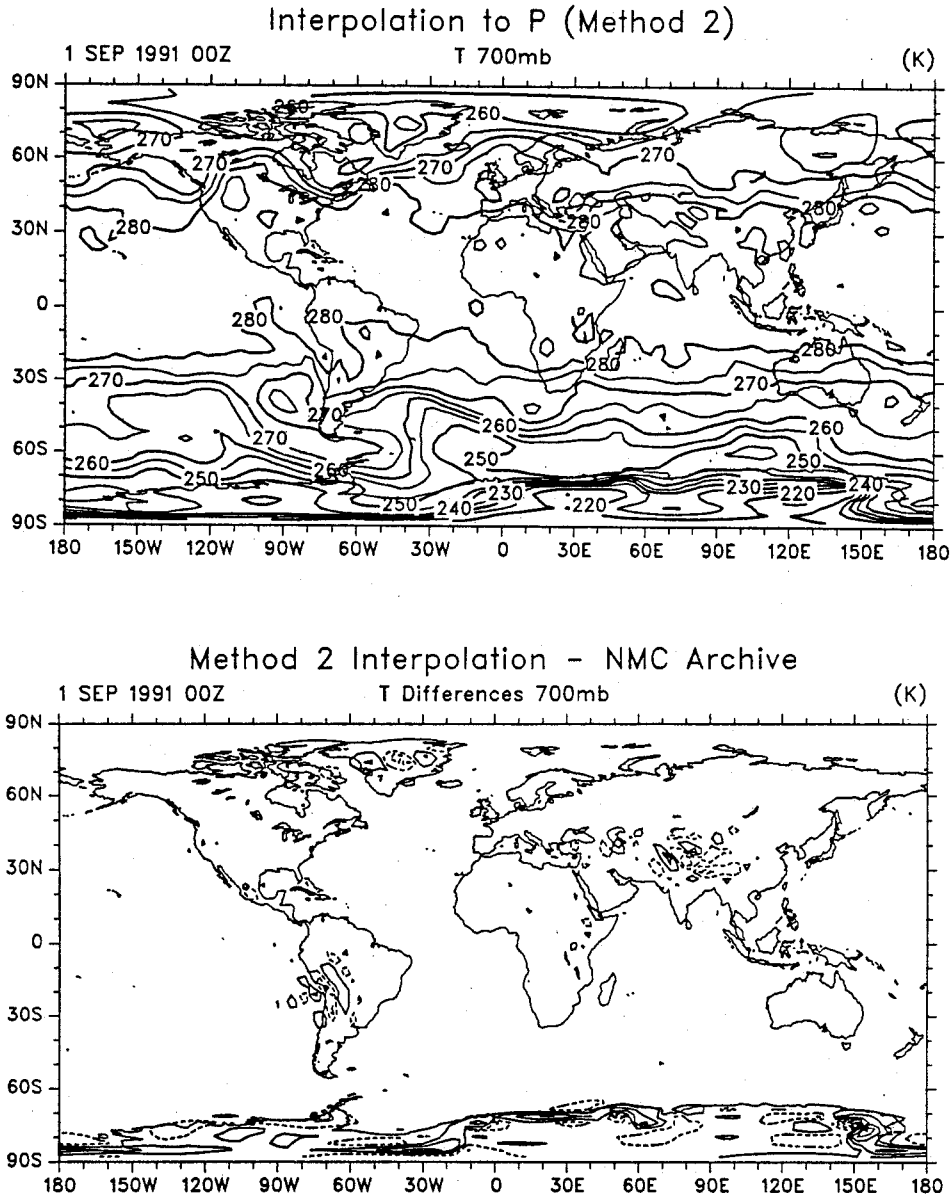

Fig. 4. As in Fig. 3 for the middle and lower panels, but with new interpolation procedures. The contour interval is 5° C in the top panel and 2° C in the lower panel, and the zero contour is omitted.

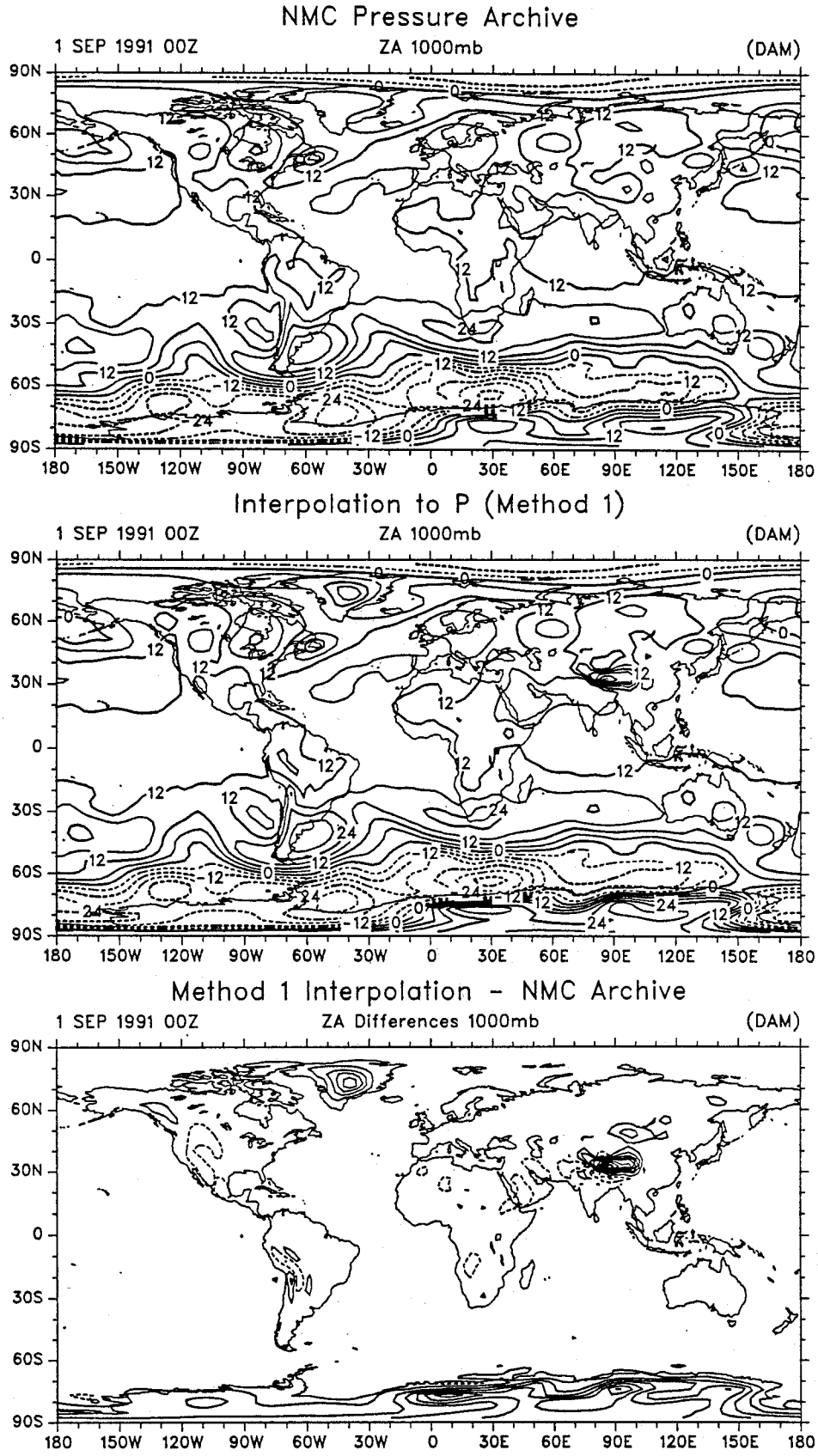

Fig. 5. For 1 September 1991 at 0000 UTC, shown are the 1000 mb gepotential height analysis from NMC, as obtained from the NMC archive (top), the corresponding field interpolated using former CCM procedures from NMC analyses on σ surfaces (middle) and their differences (bottom). The differences are derived minus archived field. The contour interval is 6 dam (60 m) in the top two panels and 3 dam (first contours ± 1.5 dam) in the bottom panel.

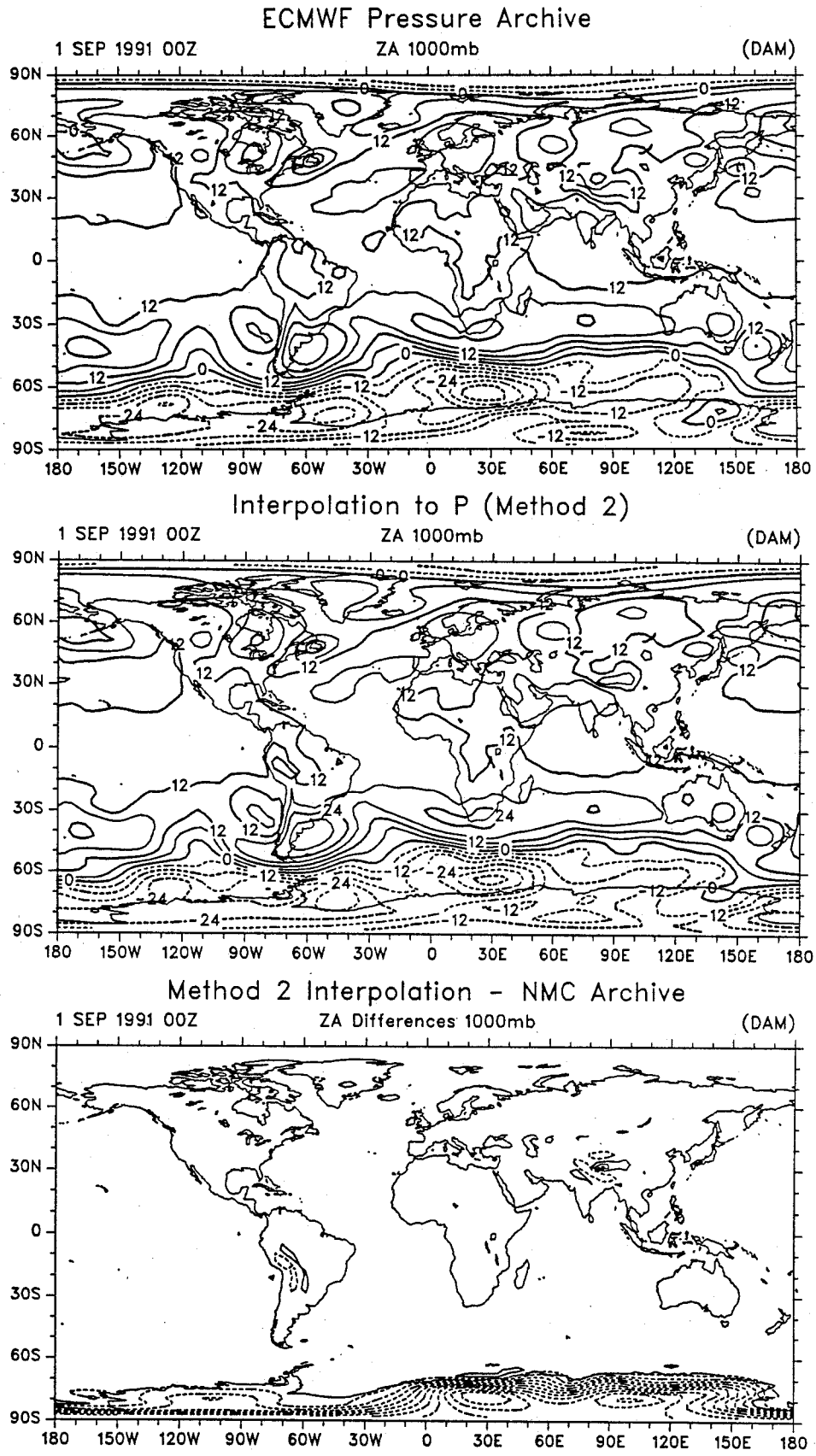

Fig. 6. For 1 September 1991 at 0000 UTC, shown are the 1000 mb gepotential height analysis from ECMWF archive (top), the field interpolated using new CCM procedures based on the ECMWF algorithm applied to NMC analyses on σ surfaces (middle) and the difference with the NMC analysis (i.e., between the middle panel and the top panel of Fig. 5) (bottom). The contour interval is 6 dam in the top two panels and 3 dam (first contours ± 1.5 dam) in the bottom panel.

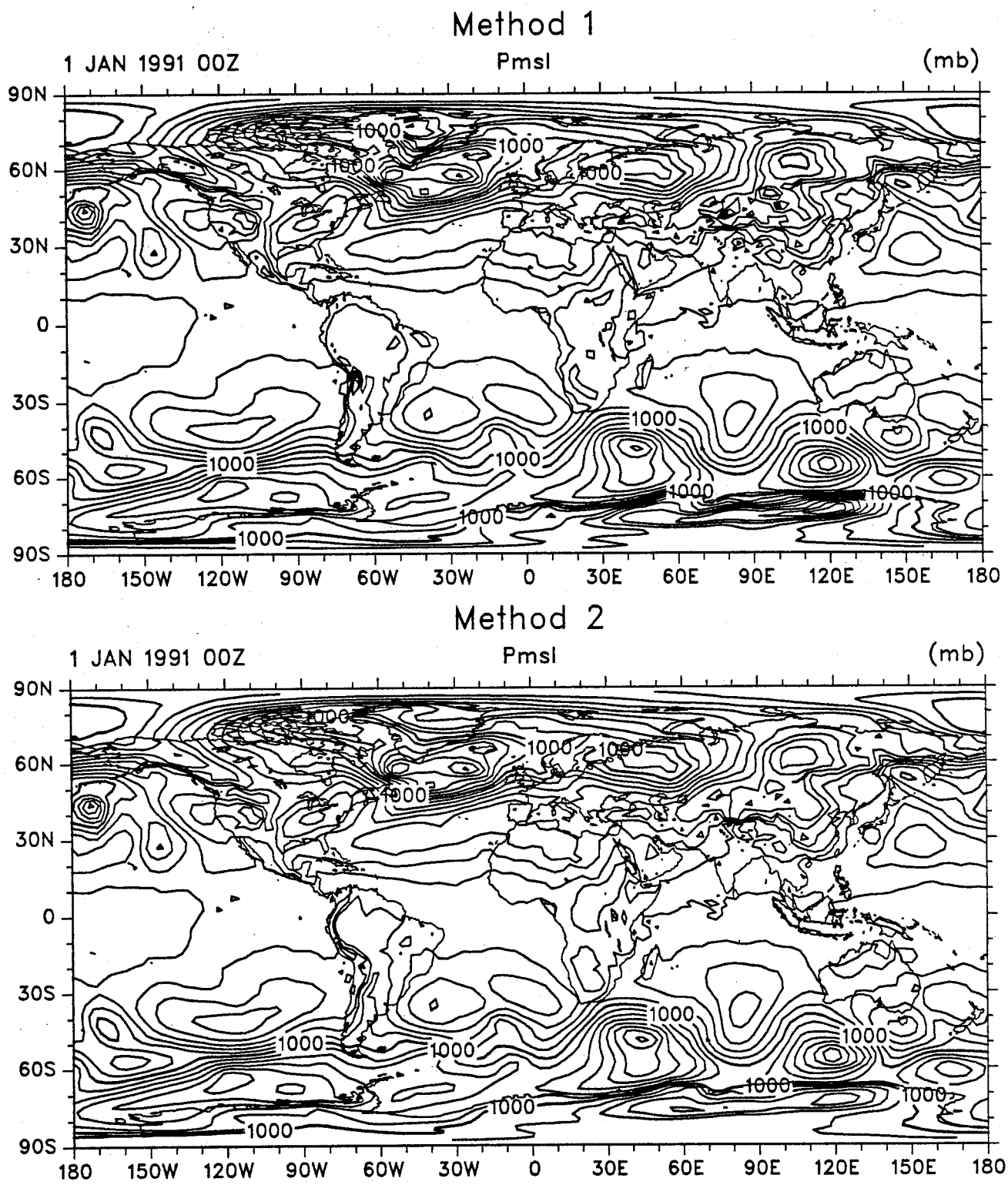

Fig. 7. Mean sea level pressure at T106 resolution with a 5 mb contour interval for 1 January 1991 at 0000 UTC from the original CCM processor algorithm (labelled method 1) (top) and from the ECMWF algorithm (labelled method 2) (bottom).

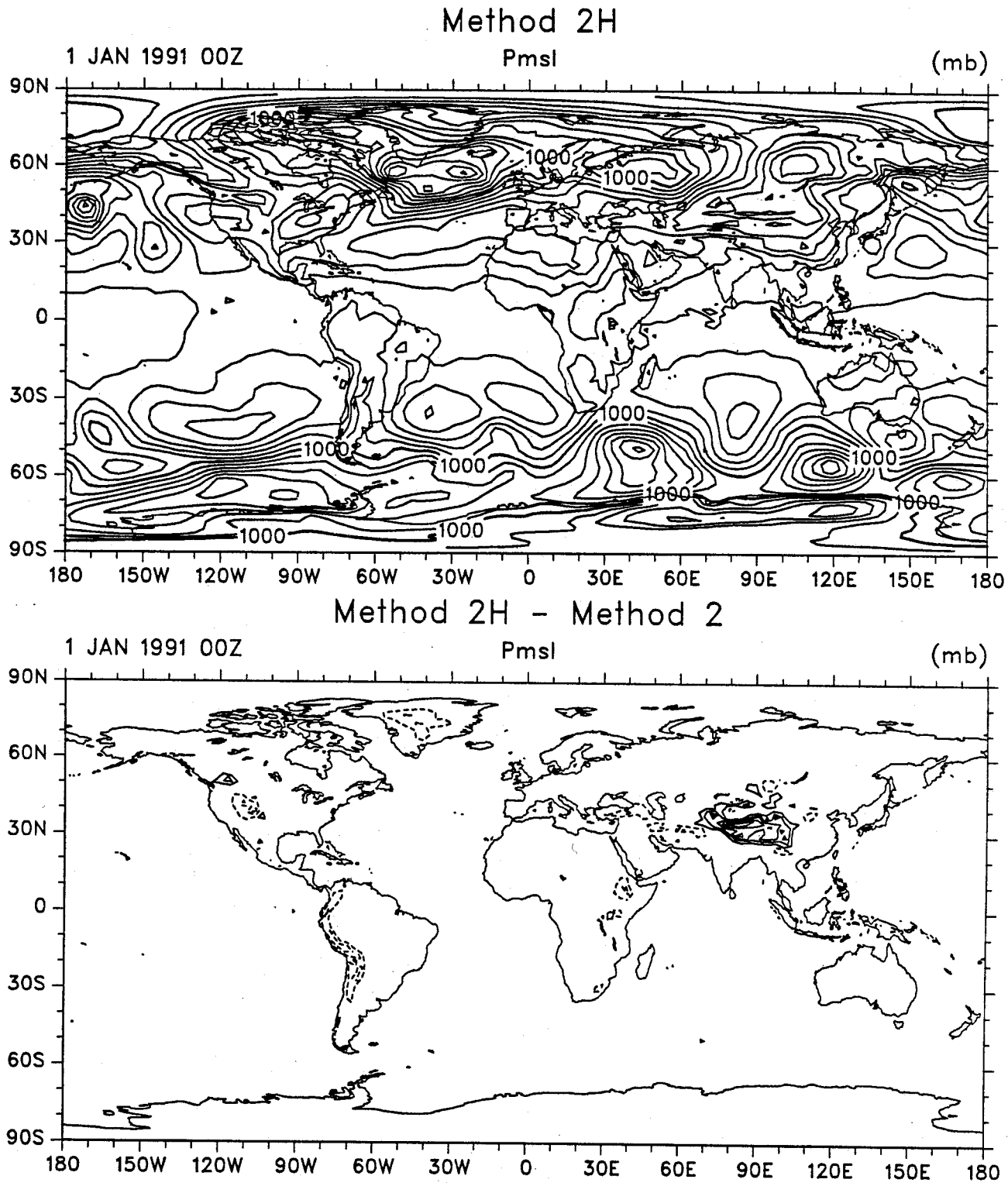

Fig. 8. Mean sea level pressure at T106 resolution for 1 January 1991 at 0000 UTC from the new full algorithm (labelled method 2H) (top) and the difference from that with the ECMWF algorithm (method 2, in Fig. 7) (bottom). The contour interval is 5 mb in the top and 4 mb in the lower panel (first contours ±2 mb).

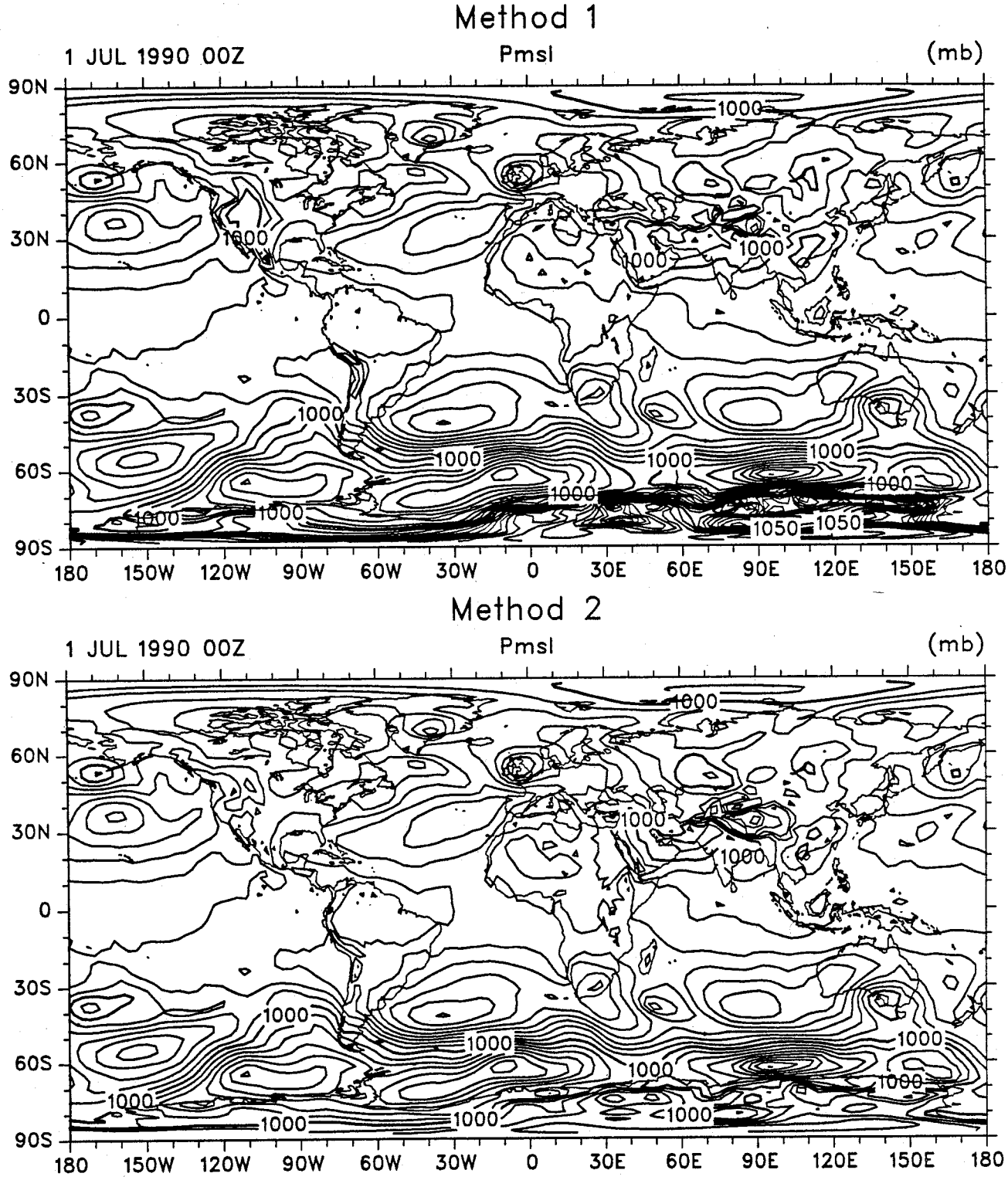

Fig. 9. Mean sea level pressure at T106 resolution with a 5 mb contour interval for 1 July 1990 at 0000 UTC from the original CCM processor algorithm (labelled method 1) (top) and from the ECMWF algorithm (labelled method 2) (bottom).

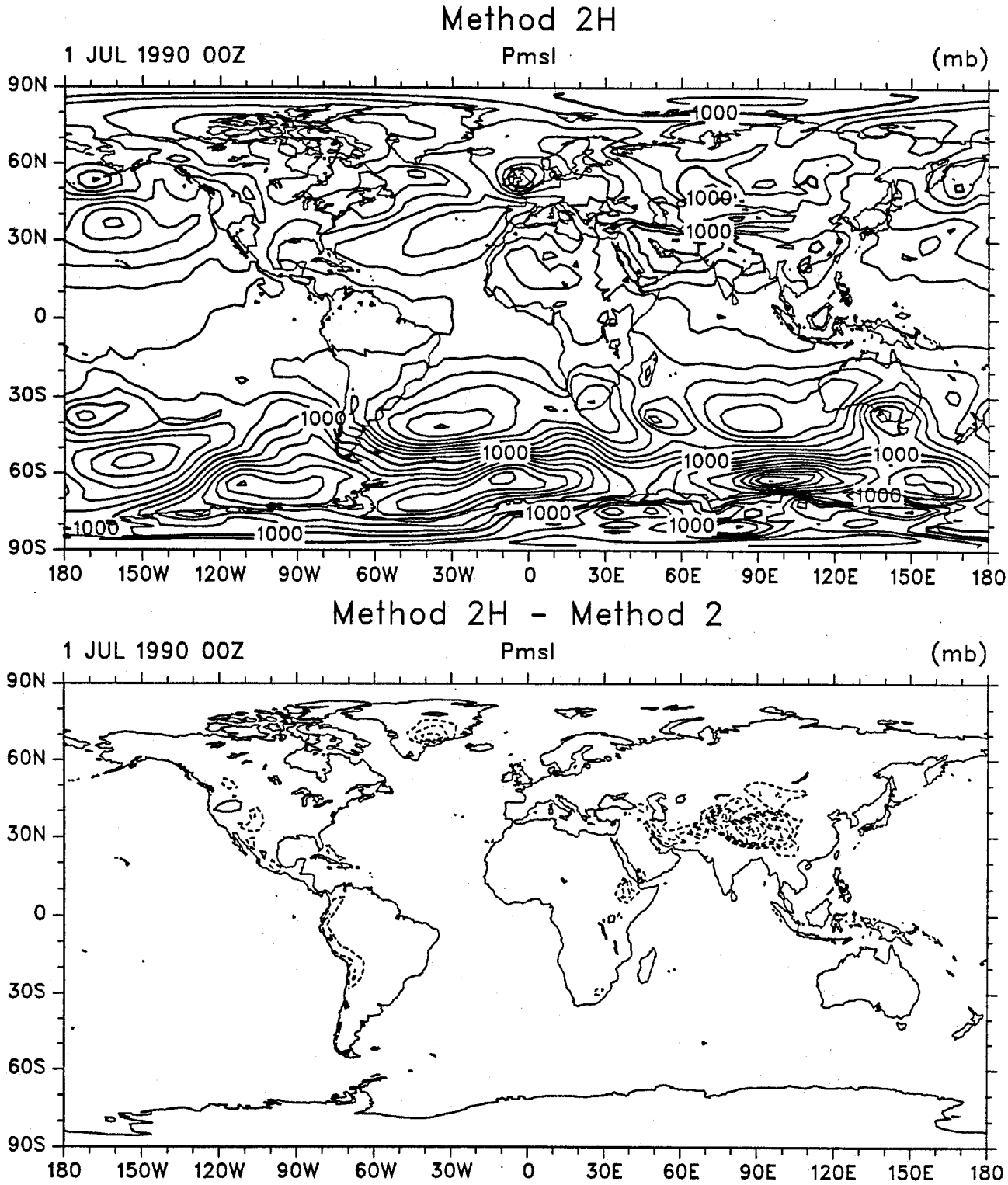

Fig. 10. Mean sea level pressure at T106 resolution for 1 July 1990 at 0000 UTC from the new full algorithm (labelled method 2H) (top) and the difference from that with the ECMWF algorithm (method 2, in Fig. 9) (bottom). The contour interval is 5 mb in the top and 4 mb in the lower panel (first contours ±2 mb).

4. Truncation on model surfaces

4.1 Model versus pressure coordinates

As noted in the introduction, a change in resolution of the analyses is often desirable but is not easily achieved on model surfaces because as the resolution changes, the vertical coordinate also changes. The problem can be illustrated by considering the horizontal gradients of any quantity A on both σ and p surfaces

$$\left.\frac{\partial A}{\partial s}\right|_p = \left.\frac{\partial A}{\partial s}\right|_\sigma + \left.\frac{\partial A}{\partial \sigma}\frac{\partial \sigma}{\partial s}\right|_p \tag{20}$$

where s is x or y. For $\sigma = \frac{p}{p_s}$, $\frac{\partial \sigma}{\partial s} = -\frac{\sigma}{p_s}\frac{\partial p_s}{\partial s}$. Consequently, the horizontal gradients or structure of the field A on p surfaces is made up of horizontal gradients of A on σ surfaces plus contributions from the product of vertical gradients of A and horizontal gradients of p_s. The latter term is very large near high orography so the nonlinear term becomes important as long as there are vertical gradients in the field A near orography.

4.2 Tests for changes in resolution: individual fields

For 1 January 1991, a number of tests have been made using the hybrid archive from ECMWF at T106 resolution. In the first case, the fields are extracted from the archive on the hybrid surfaces at full resolution, interpolated or extrapolated to p surfaces and then spectrally truncated to lower resolution, T63 or T42 for purposes of illustration (see Trenberth and Solomon 1993 for spectral truncation on constant pressure surfaces). This is referred to as the "HPTxx" (Hybrid interpolated to p then Truncated to Txx) field. In the second case, the latter two steps are reversed, so it is referred to as the "HTxxP" case. The full fields on the hybrid surfaces are first truncated to lower resolution (T63 or T42), then vertically interpolated to p surfaces, and finally truncated again. The vertical interpolation typically adds structure on the grid scale so that an additional truncation is necessary to make the fields consistent with the new resolution for comparison with the first case.

Note that in all cases in dealing with p_s, in the original spectral archive, the field $\ln p_s$ is the preferred variable, and all truncations were made using spherical harmonic series of the latter, not p_s.

Figures 11–17 show the results for geopotential height z and zonal wind u at 700 mb

and temperature T at 850 mb. Because of the nonlinear term in (20), the simple reversal in order of operations does not give the same result. The correct solution is the HPT case and the difference is a measure of how large the errors introduced by truncating directly on the hybrid surfaces are. Firstly, the results are given for T63 truncation and the total field is shown (Fig. 11) along with the differences at T63 resolution (Fig. 12) and at T31 resolution (Fig. 13). Fig. 16 shows the corresponding spectra for all three fields giving the power versus total wavenumber n. In all cases, the largest errors are at the truncation resolution at wavenumber 63 and are physically located in the immediate vicinity of the mountains. Typical magnitudes are 20 m (range -50 to +60) for z, 1 m s^{-1} (range -2 to +3) for u and 2°C (range -5 to 10) for T at T63, and 4 m for z, 0.3 m s^{-1} for u and 0.5°C for T at T31 resolution.

The second set of figures (Figs. 14, 15 and 17) shows the corresponding results for truncation at T42 on the hybrid surfaces but with differences at T42 and T21 resolution with typical magnitudes of 25 m (range -70 to +80) for z, 1.5 m s^{-1} (range -4 to +5) for u and 1.5°C (-5 to +8) for T at T42, and 6 m for z, 0.5 m s^{-1} for u and 0.5°C for T at T21. Clearly the errors at T42 are larger on all scales and the spectra reveal that the error in the smallest scales is about the same regardless of the truncation (i.e., the errors at wave 63 are about the same as those at wave 42 in the corresponding T63 and T42 truncations). The acceptability of these errors will depend on application.

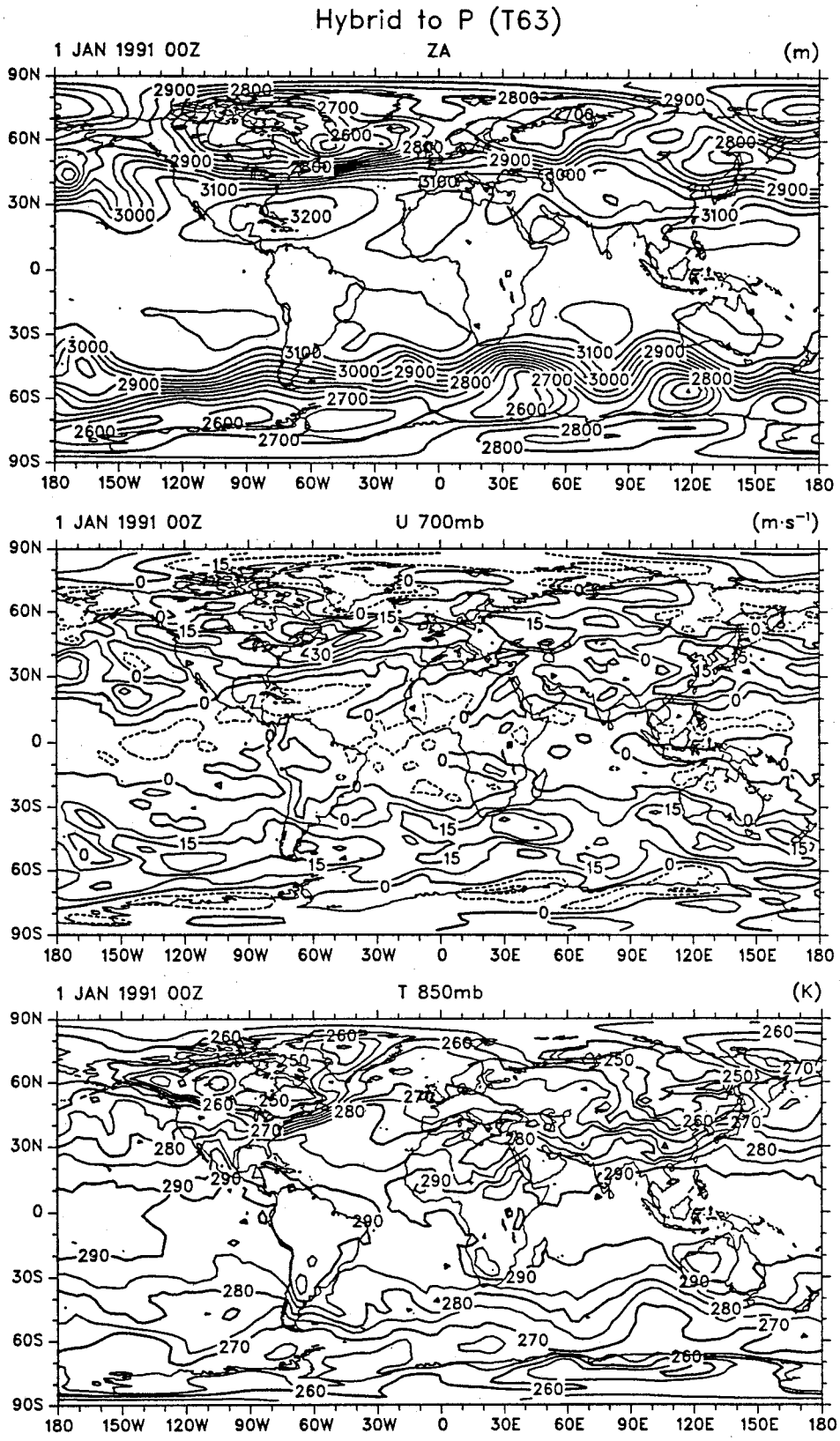

Fig. 11. Fields of z at 700 mb, contour interval 50 m (top), u at 700 mb, contour interval 7.5 m s^{-1} (middle), and temperature at 850 mb, contour interval 5 K. The fields are for 1 January 1991 and have been interpolated from the original hybrid level archive to pressure levels and then truncated (HPT63) at T63.

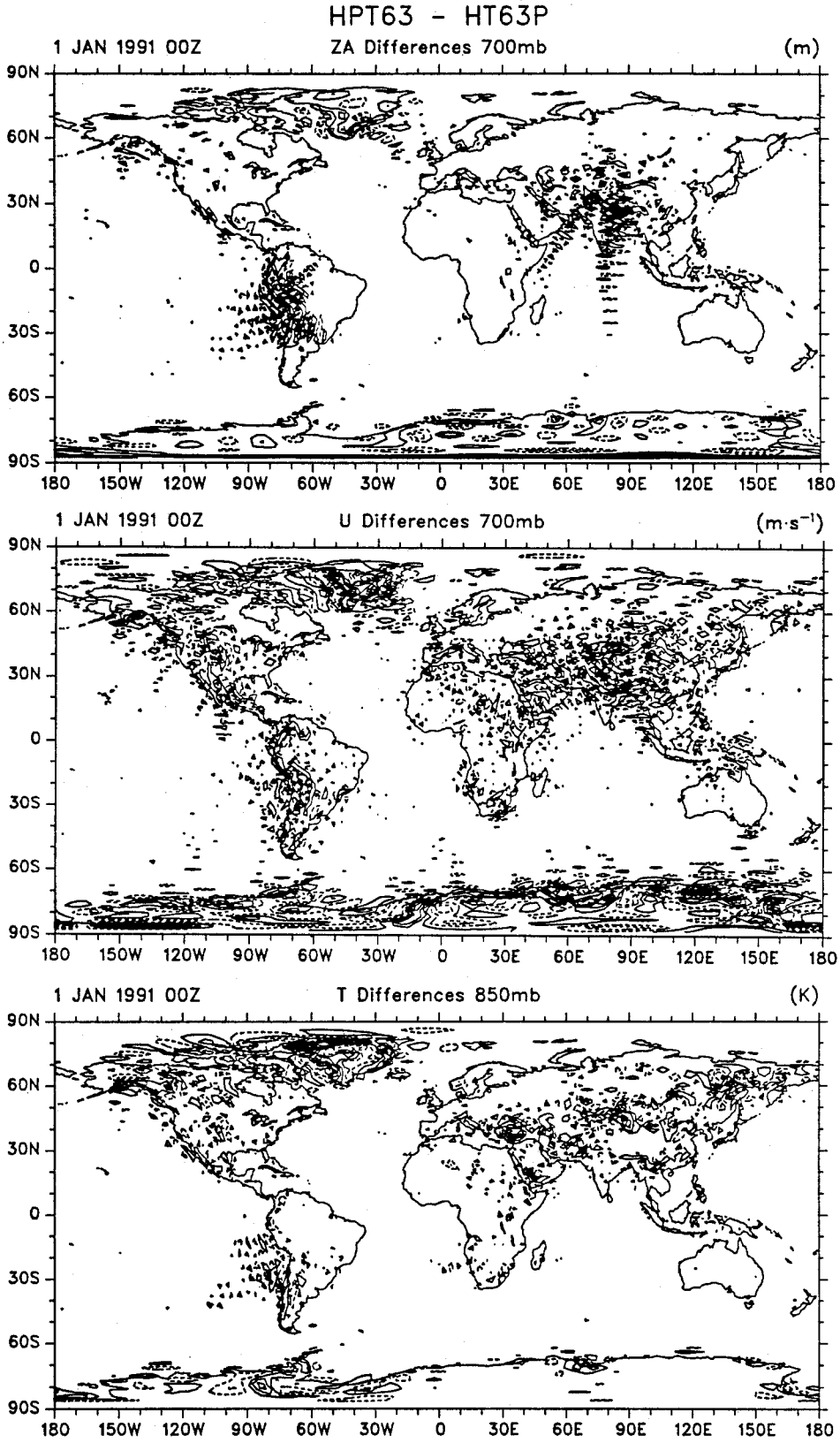

Fig. 12. Difference fields of z at 700 mb, contour interval 5 m (top), u at 700 mb, contour interval 0.5 m s^{-1} (middle), and temperature at 850 mb, contour interval 1 K. The fields are for 1 January 1991 and are differences HPT63 – HT63P, where HT63P refers to hybrid, truncated at T63, then interpolated to pressure and HPT63 refers to hybrid, interpolated to pressure, then truncated at T63. Contours are chosen so that the zero contour is not plotted.

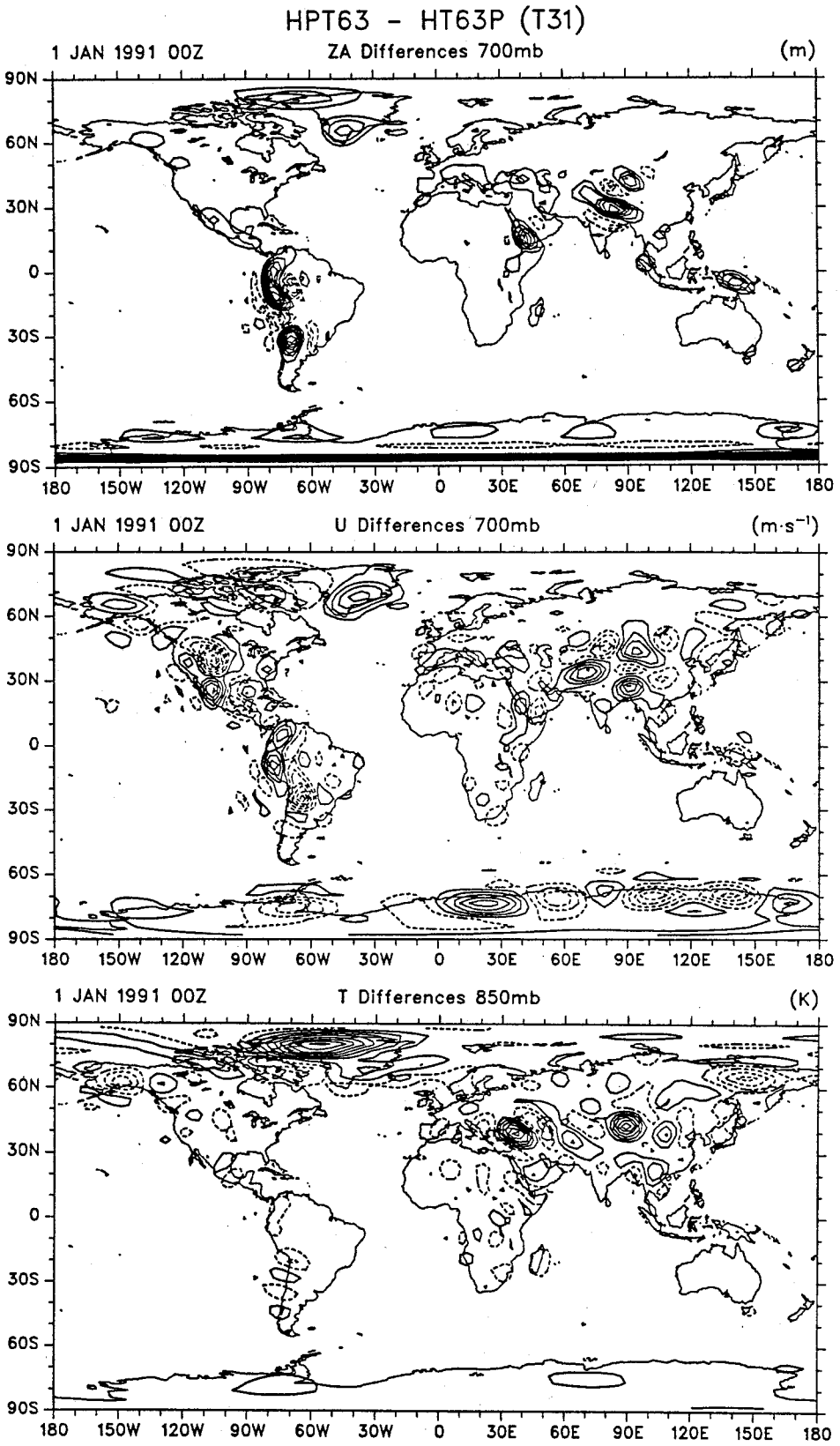

Fig. 13. As in Fig. 12 except the results have been truncated at T31 and the contour intervals are 1 m, 0.1 m s^{-1} and 0.2 K.

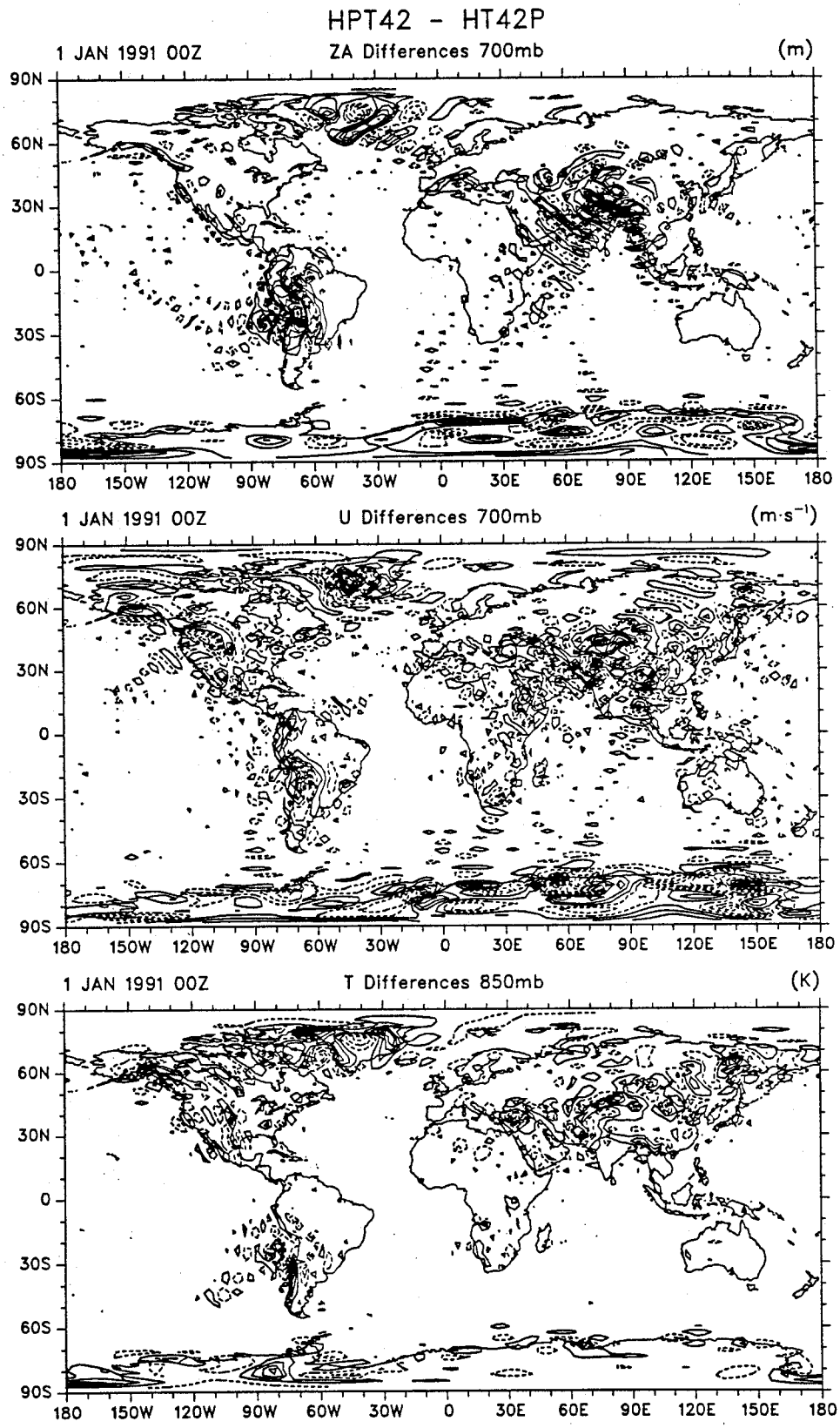

Fig. 14. As in Fig. 12 except truncation is at T42. Contour intervals are 5 m, 0.5 m s^{-1} and 1 K.

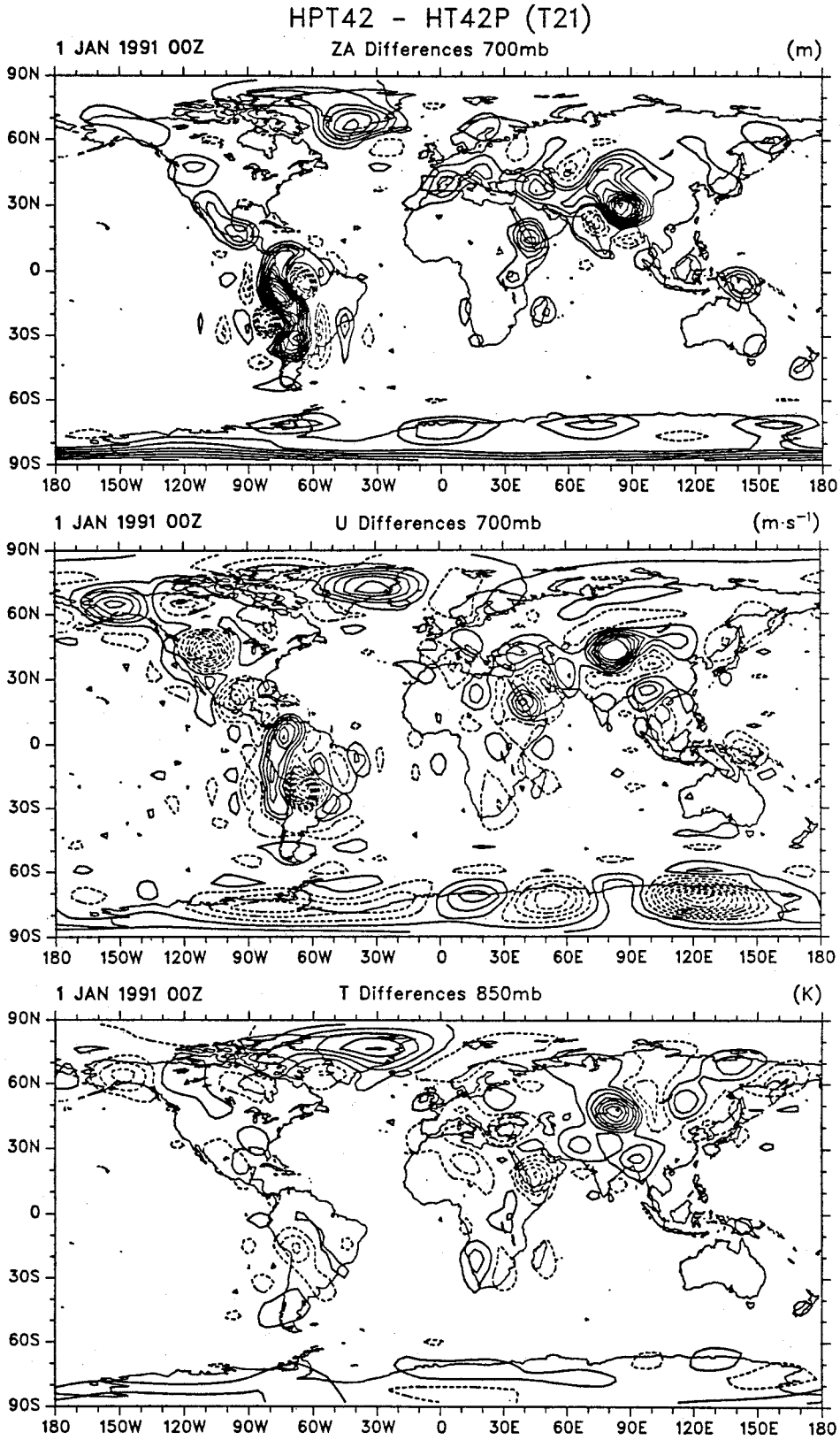

Fig. 15. As in Fig. 14 except the results have been truncated at T21. Contour intervals are 1 m, 0.1 m s^{-1} and 0.2 K.

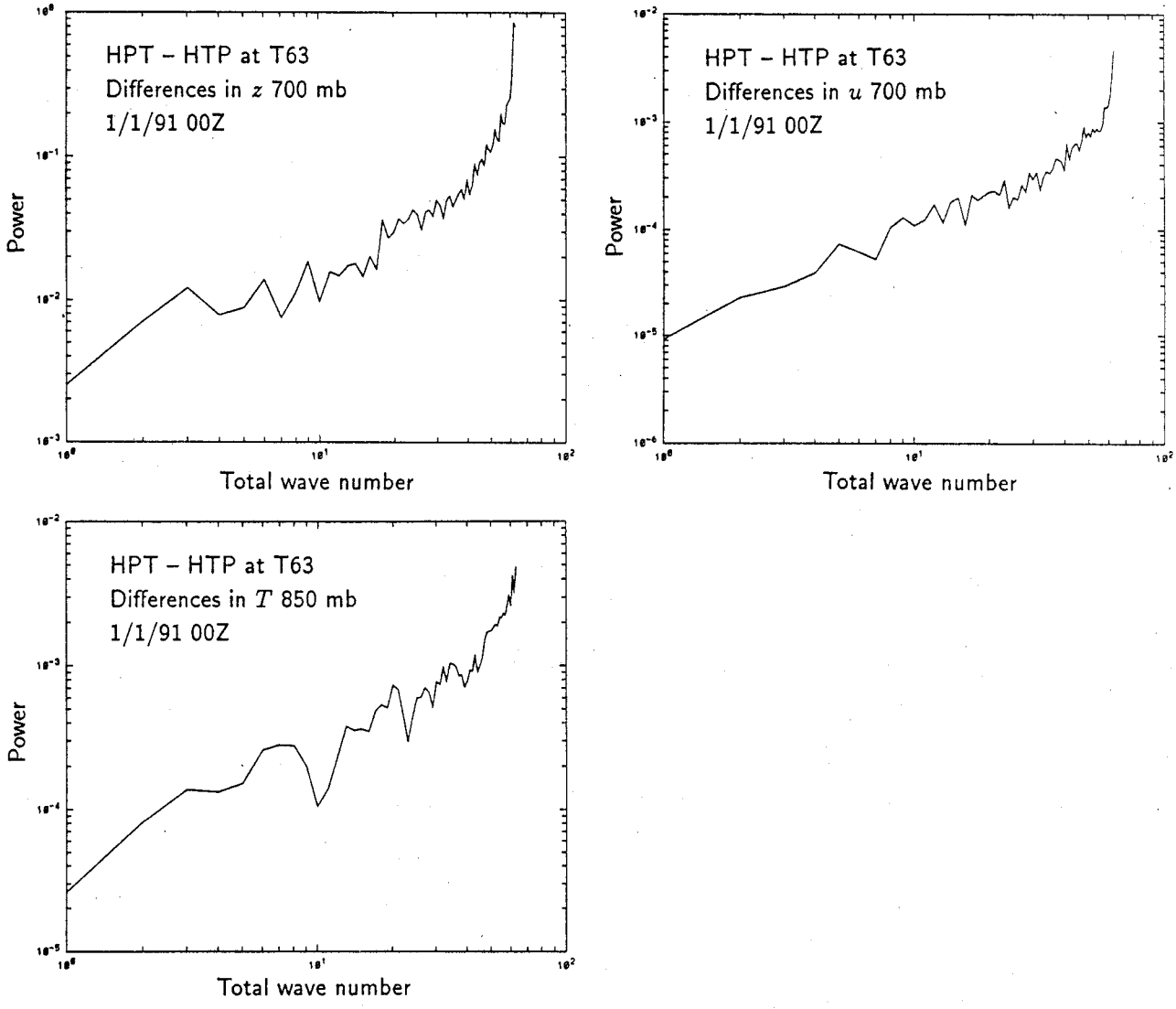

Fig. 16. Spectra of the difference fields shown in Fig. 12. The coordinates are logarithmic and the abscissa includes points up to wave 63.

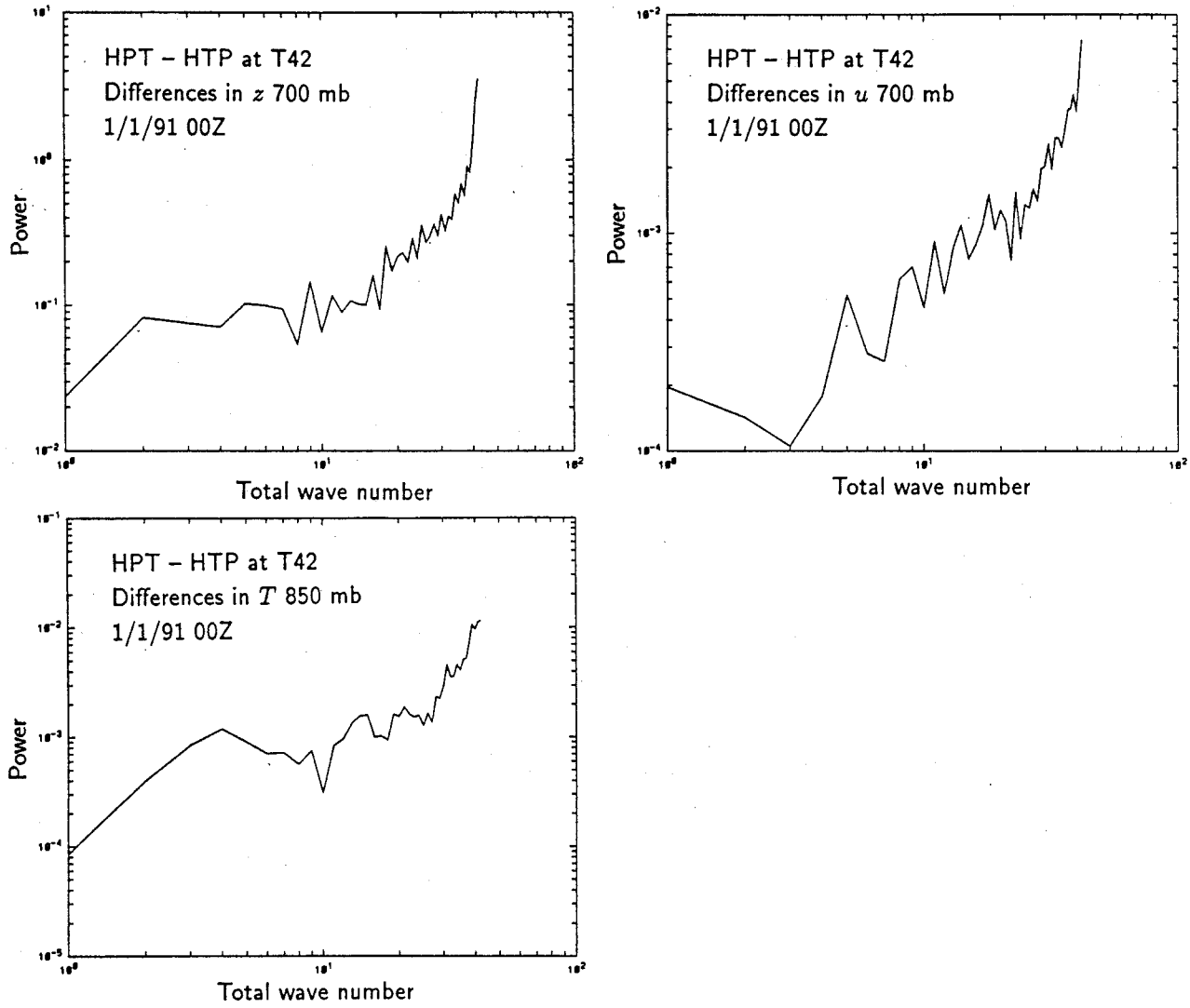

Fig. 17. Spectra of the difference fields shown in Fig. 14. The coordinates are logarithmic and the abscissa includes points up to wave 42.

5. Time averages on model surfaces

Given any variable x on model surfaces x_η or interpolated to pressure x_p, we define the time average by an overbar

$$\overline{x} = \frac{1}{N}\sum_{n=1}^{N} x_n \ . \tag{21}$$

1. This can be performed on pressure surfaces to give $\overline{x}_p$, or
2. it may be performed on model (η) surfaces to give $\overline{x}_\eta$, in which case it applies on $\overline{\eta}$ surfaces presumably, and could be interpolated to p using these redefined surfaces, or
3. it can factor in a mass weighting by recognizing that the level value is also used as representative of the layer $\Delta\eta$. In this latter case the mass weighting is proportional to

$$x_\eta \frac{\partial p}{\partial \eta}\Delta\eta = x_\eta \Delta p \tag{22}$$

where Δp is the thickness of the layer and we have ignored the $\frac{1}{g}$ factor.

In this latter case we can define a time average $\tilde{x}_\eta$

$$\tilde{x}_\eta = \frac{\overline{x\,\Delta p}}{\overline{\Delta p}} \tag{23}$$

This has the advantage that it can be directly related to any layer or column integral quantity by weighting it by $\overline{\Delta p}$ which is not a function of time. Again we can interpolate results to p using the time average coordinate.

$\overline{x_\eta}$ and $\overline{x_p}$ are fundamentally different and do not relate to one another. $\overline{x_\eta}$ ignores covariances with p_s. For p coordinates, a Δp can be added at any point in the calculation as Δp is constant, so layer or column integrals are easily achieved. From this standpoint $\tilde{x}_\eta$ from (23) would seem to be preferable to $\overline{x}_\eta$.

Technically, therefore, the meaning of a time average relates to the coordinate system in which it is obtained and it may not be possible to strictly relate the time averages in one coordinate with those in another. Practically, however, we can ask how large the differences are between the three definitions given above. Perhaps fortunately, the differences among the three are quite small. This is illustrated below for the month of January 1991 for 0000 UTC every second day for the month, so that there are 15 values going into the monthly

mean fields.

Figure 18 shows, for 850 mb, differences between $\overline{T}_\eta$ and $\overline{T}_p$, i.e., the time average of T in hybrid coordinates, interpolated to p, versus the time average of T in pressure coordinates, with the result truncated at T31 resolution. In the bottom panel is shown the corresponding difference between $\overline{T}_\eta$ and $\widetilde{T}_\eta$. All differences are small and range up to ± 0.3 K in the top panel and ± 0.1 K in the bottom panel. These results are typical of other levels in the vertical. Similarly, for geopotential height (not shown), differences between the methods of time averaging are small, typically about 1 m at 500 mb and with a maximum value of -3 m near Iceland for the Δp weighting case (cf. Fig. 20).

Figures 19 and 20 show the corresponding differences for the u and v fields at 700 mb. In both cases the contour interval is 0.05 m s^{-1} and values range up to about ± 0.2 m s^{-1}. The patterns are interesting, however, and relate to the covariance of u and v with p_s that arise because of storm tracks. Because baroclinic storm systems slope westward with height, poleward winds at 700 mb (v positive in the northern hemisphere (NH) and negative in the southern hemisphere(SH)) are closely associated with low pressures (Trenberth 1991b) in eastward moving storms. The differences between $\widetilde{v}_\eta$ and $\overline{v}_\eta$ are easiest to interpret as $\widetilde{v}_\eta \overline{\Delta p} = \overline{v_\eta \Delta p} = \overline{v}_\eta \overline{\Delta p} + \overline{v'_\eta \Delta p'}$, where $\Delta p'$ is proportional to p'_s. Thus the last term here is negative in the NH and positive in the SH in the storm tracks, giving rise to the difference pattern seen in Fig. 20. In Fig. 19, much the same pattern emerges but it is even stronger. Equivalent differences at other levels are mostly smaller than at 700 mb.

The conclusion from this section is that while the meaning of a time average in different coordinates is not the same and it is not always possible to relate the time average in p to that in η, in practical terms, the differences are quite small and probably negligible for most purposes.

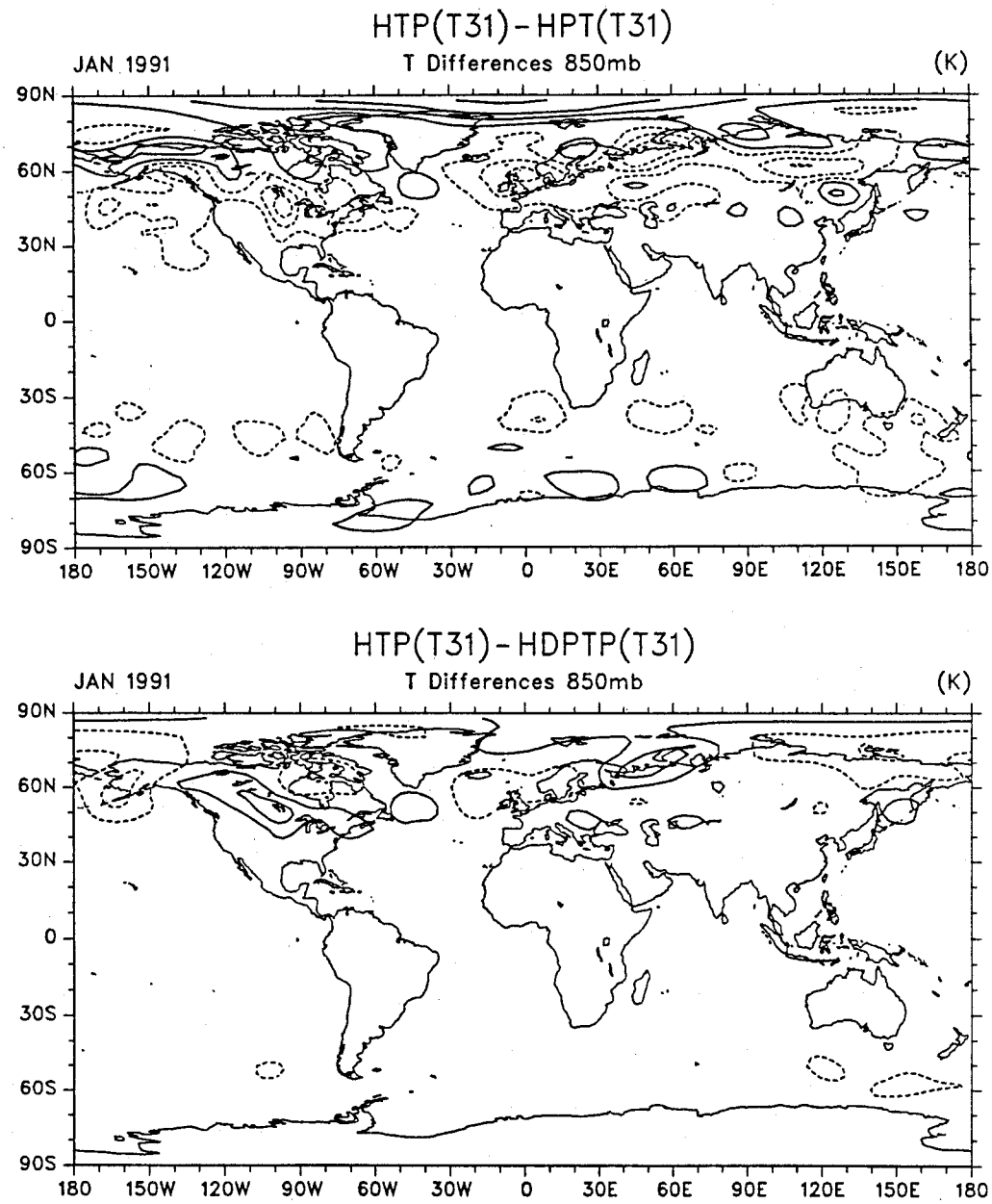

Fig. 18. At 850 mb for January 1991, differences between $\overline{T}_\eta$ (the time average of T in hybrid coordinates, interpolated to p) and $\overline{T}_p$ (the time average of T in pressure coordinates) with the result truncated at T31 resolution (top), and the corresponding difference between $\overline{T}_\eta$ and $\tilde{T}_\eta$ (which has the Δp weighting) (bottom). The contour interval is 0.1 K (top) and 0.05 K (bottom) with negative values dashed and contours chosen so the zero contour is not plotted.

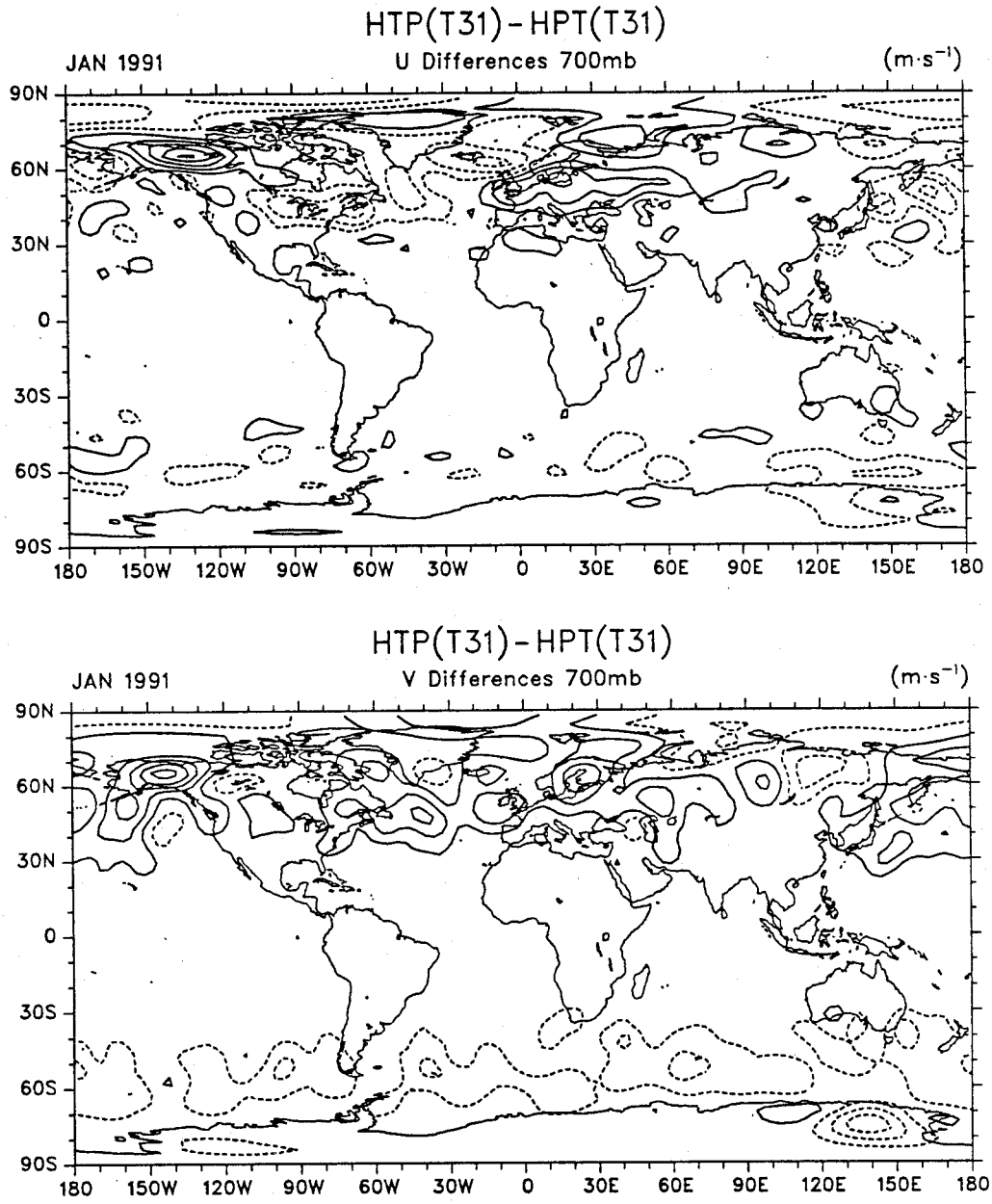

Fig. 19. At 700 mb for January 1991, differences between $\overline{u}_\eta$ (the time average in hybrid coordinates, interpolated to p) and $\overline{u}_p$ (the time average in pressure coordinates) with the result truncated at T31 resolution (top), and the corresponding difference for v (bottom). The contour interval is 0.05 m s^{-1} with negative values dashed and contours chosen so the zero contour is not plotted.

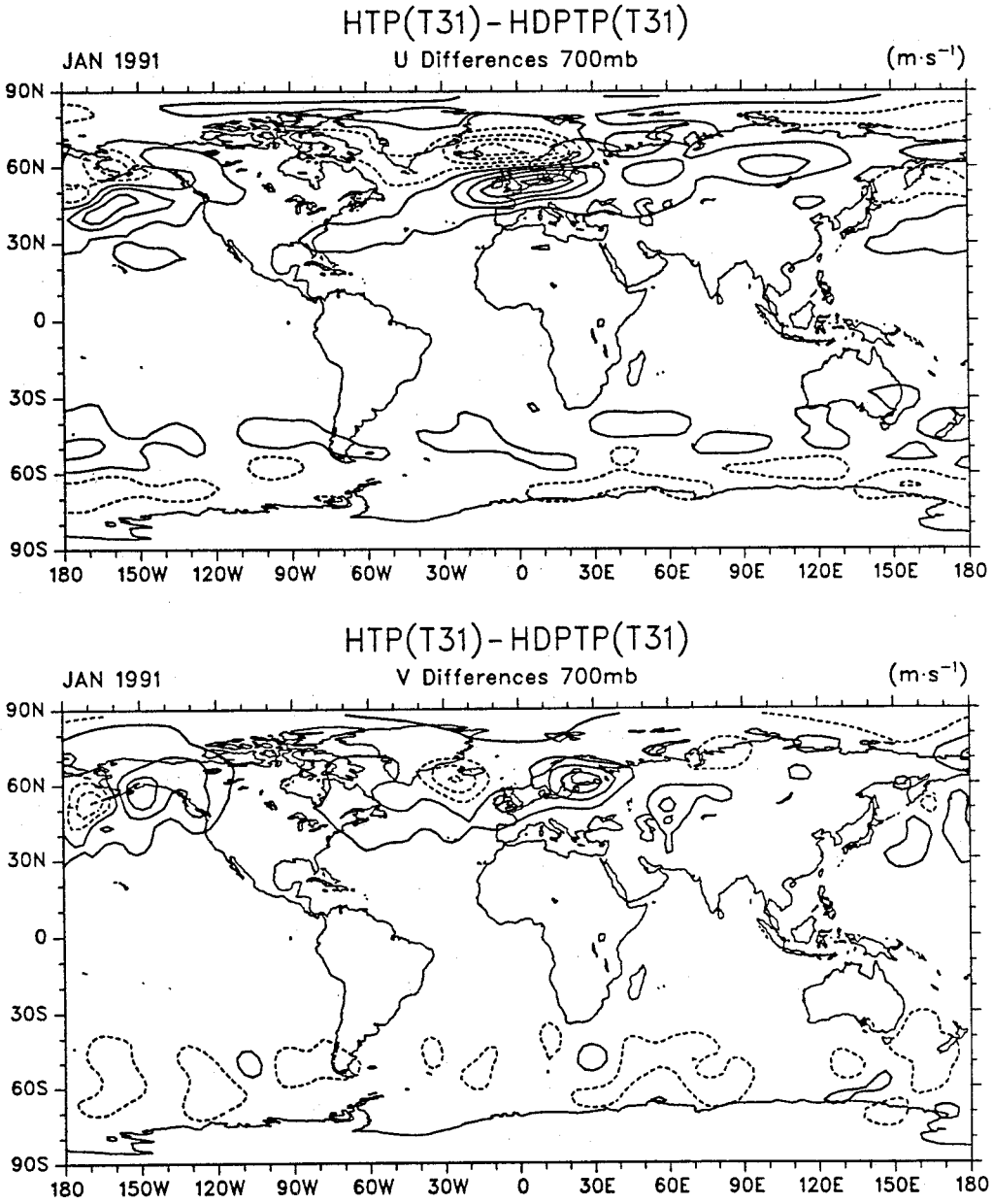

Fig. 20. At 700 mb for January 1991, differences between $\overline{u}_\eta$ (the time average in hybrid coordinates, interpolated to p) and $\tilde{u}_\eta$ (the time average of u weighted with Δp in hybrid coordinates, interpolated to p) with the result truncated at T31 resolution (top), and the corresponding difference for v (bottom). The contour interval is 0.05 m s^{-1} with negative values dashed and contours chosen so the zero contour is not plotted.

6. The heat budget: tests for changes in resolution

To further test the importance of the truncation errors for budget applications, it was deemed necessary to determine whether the effects might become magnified through non-linear terms. Accordingly, a test has been made for the thermodynamic equation.

The tests are made for January 1991. Because of the difficulty in handling T106 data, the test uses analyses from only 0000 UTC every second day for the month, so that there are 15 values going into the monthly mean fields.

In p coordinates the thermodynamic equation may be written as:

$$\frac{\partial T}{\partial t} = -\nabla \cdot \mathbf{v}T + T\delta - \omega\frac{\partial T}{\partial p} + \kappa\frac{\omega T}{p} + \frac{Q}{c_p} \tag{24}$$

where $\delta = \nabla \cdot \mathbf{v}$ is the divergence and other notation is standard. Note the first two terms on the right-hand-side (rhs) together constitute the horizontal advection term, but are written in this form for purposes of evaluation using spectral methods.

In hybrid η coordinates, where $p(\eta, p_s) = A(\eta) + B(\eta)p_s$ the thermodynamic equation takes the form

$$\frac{\partial T}{\partial t} = -\mathbf{v} \cdot \nabla T - \dot{\eta}\frac{\partial T}{\partial \eta} + \kappa\frac{\omega T}{p} + \frac{Q}{c_p} \tag{25}$$

and this is written

$$\frac{\partial T}{\partial t} = -\nabla \cdot \mathbf{v}T + T\delta - \dot{\eta}\frac{\partial p}{\partial \eta}\frac{\partial T}{\partial p} + \kappa\frac{\omega T}{p} + \frac{Q}{c_p} \tag{26}$$

see Hack et al. (1993). It is important to note that while several terms look very similar, (e.g., $\nabla \cdot \mathbf{v}T$) the divergence operator in the first case, Eq. (24), is on constant pressure surfaces, and in the second case, Eq. (26), is on the hybrid surfaces.

The vertical advection term is the product of a vertical velocity ($\dot{\eta}\partial p/\partial \eta$) and the vertical derivative of a field ($\partial T/\partial p$). The fields are defined at layer midpoints k, where k is the vertical index. The vertical velocity is defined in terms of vertical integrals of fields and is taken to interfaces at levels $k + 1/2$. The vertical derivatives are also naturally taken to interfaces, so the product is formed there and the adjacent interface values of the products are averaged to give a midpoint value. It is the definition of the average which must be correct in order to conserve kinetic energy under vertical advection. Thus, as noted in Hack et al. (1993) (in their eq. 3.a.61 and 3.a.62), the finite difference form of the vertical advection

term in (26) is written as

$$\left(\dot{\eta}\frac{\partial p}{\partial \eta}\frac{\partial T}{\partial p}\right)_k = \frac{1}{2\Delta p_k}\left[\left(\dot{\eta}\frac{\partial p}{\partial \eta}\right)_{k+1/2}(T_{k+1}-T_k) + \left(\dot{\eta}\frac{\partial p}{\partial \eta}\right)_{k-1/2}(T_k - T_{k-1})\right], \tag{27}$$

$$\Delta p_k = p_{k+1/2} - p_{k-1/2}. \tag{28}$$

Accordingly, for comparison purposes, the formulation of the corresponding term in p coordinates $\omega\frac{\partial T}{\partial p}$ is given as

$$\omega\frac{\partial T}{\partial p} = \frac{1}{4\Delta p_k}\left[(\omega_{k+1}+\omega_k)(T_{k+1}-T_k) + (\omega_k+\omega_{k-1})(T_k - T_{k-1})\right] \tag{29}$$

so that we have averaged the ω values at levels above and below to give mid-point values. It is also worth noting that for consistency, we have recomputed ω. Although values were provided by ECMWF, we find significant differences, mostly in the smaller scales and especially around orography. On examining the postprocessing formulae used at ECMWF it is not clear that the archived values are correct. Some of the differences may arise from use of p_s in the postprocessing whereas $\ln p_s$ is the variable used by the model and in our processing.

We have then computed the three terms, (i) the advection term, consisting of the first two terms on the rhs of each equation, (ii) the vertical advection terms as given in (27) and (29), (iii) the $\kappa\frac{\omega T}{p}$ terms and (iv) their sum, as an approximation to Q/c_p. All terms are converted into units of K/day.

Several different heat budget calculations have been performed to test the impact of interpolation and truncation.

1. The full calculation in model coordinates (T106 hybrid), with the results interpolated to p using a lnp interpolation each day, then time averaging on p surfaces, and finally truncation to T31.
2. T106 hybrid, interpolated to p, then do the calculation in p coordinates, time average, then truncate results to T31.
3. T106 hybrid, truncate to T63, calculate results, interpolate to p, time average, then truncate to T31.
4. T106 hybrid, truncate to T42, calculate results, interpolate to p, time average, then truncate to T31.

5. T106 hybrid, interpolate to p, truncate to T63, calculate results, time average, then truncate to T31.
6. T106 hybrid, interpolate to p, truncate to T42, calculate results, time average, then truncate to T31.
7. T106 hybrid, calculate results at full resolution, time average, interpolate to p, then truncate to T31.
8. T106 hybrid, calculate results at full resolution, weight by Δp, time average, interpolate to p, then truncate to T31.

There is no single "correct result". All interpolations to p are at 50 mb vertical resolution, so the latter is not an issue. All results are finally truncated to T31 so that the larger scales of interest are emphasized. Result 1 is one version of truth but suffers from interpolation of the results to p. Result 2 shows the most accurate result that can be achieved using p coordinates. The difference between 1 and 2 reveals the effects of vertical interpolation at different times in the calculation and for extrapolating below ground.

Results 5 and 6 are also in p coordinates where truncation is well defined, and results should be little changed from 2 unless nonlinear interactions of high wavenumber project onto the lower wavenumbers. Results 3 and 4 test the impact of the ill-posed truncation in hybrid coordinates at different resolutions (T63 and T42) on results at T31 resolution.

Results 7 and 8 are alternatives to result 1 where the time averaging is performed on η surfaces. From section 5, we anticipate that the ordering of the time averaging will not make a large difference, but these results check this aspect.

Results for each term will be presented from calculations 1 and 2, to show the effects of the coordinate system change and illustrate how the terms compensate one another, and results for the sum, the total heating, are given for the other calculations.

6.1 Heat budget results from changes in resolution

The terms in the Eq. (24) are labeled as follows: $ADV = \nabla \cdot \mathbf{v}T - T\delta$, $WDT = \omega \frac{\partial T}{\partial p}$, $KWT = -\kappa \frac{\omega T}{p}$ and $\frac{Q}{c_p}$. For Eq. (26), the term $EDT = \dot{\eta} \frac{\partial p}{\partial \eta} \frac{\partial T}{\partial p}$ is included, otherwise the same labels are used (although the terms are computed on hybrid, not p coordinates).

Figure 21 shows the ADV, WDT, and KWT terms at 700 mb from the full calculation

in p coordinates. The corresponding terms in the hybrid coordinate system are shown in Fig. 22, and their difference is given in Fig. 23. As is typical at all levels, the differences reveal the effects of the distortion of the hybrid coordinate system over the mountains, so that differences there are large and of one sign for ADV, but are equally large and of opposite sign for WDT versus EDT. Differences in KWT are small except where values are extrapolated below ground. The result from the hybrid calculation is more extreme and seems less desirable in this case.

The sum of these terms at 700 mb is given in Fig. 24 and for 300 mb in Fig. 25. The difference map in the total heating shows how effective the cancellation apparent in Figs. 21 and 22 has been. Differences are large at 700 mb near high mountains where extrapolation below ground has occurred. At 300 mb differences range from -2 to 3°/day. A pattern is apparent in the difference field at all levels with a wave 2 structure (mostly negative over the Pacific and Africa, but positive over South America and Asia. This structure comes mostly from the $WDT - EDT$ term and evidently is related to the semidiurnal tide which has somehow rectified the product to produce a systematic component of about 0.5°/day amplitude. Otherwise the differences are quite noisy and largest near mountains, even in the free atmosphere. Thus the lower panels in Figs. 24 and 25 show the magnitude of errors from vertical interpolation. Zonal averages (not shown) reveal differences of $\sim$0.1 K/day.

In pressure coordinates, Fig. 26 shows the effects of truncation at T42 of each field before the terms are evaluated. Shown at T31 resolution are the differences from the top panels in Fig. 24 at 700 mb and Fig. 25 at 300 mb. These differences can only arise from nonlinear effects of waves shorter than T42 projecting onto lower wavenumbers. At 300 mb, differences are at most 0.5°/day with fairly small scale structure and typical values of 0.1 to 0.2°/day. At 700 mb, differences are similar in magnitude over the oceans but an order of magnitude larger although confined to mountainous areas where extrapolation below ground is a factor.

Figure 27 shows the result of the calculation with the fields first truncated at T42 in hybrid coordinates. As noted earlier, this is ill posed because of the coordinate change (e.g., see Fig. 12). Shown in each panel are differences from the full calculation in the second panels of Figs. 24 and 25. As expected, differences are greatest in the vicinity of mountains

but propagate out from those areas. Differences range from -3.25 to 1.75 K/day at 300 mb and -12.5 to 11.5 K/day at 700 mb. Such large magnitudes are judged unacceptable.

Figure 28 shows the result corresponding to that in Fig. 27 but using T63 truncation instead. Errors are reduced at both levels and range from -0.63 to 0.63 at 300 mb and -8 to 5 K/day at 700 mb, and are confined to the high mountain areas. These errors are comparable to or less than the discrepancies arising from vertical interpolation and are therefore judged to be more acceptable. Accordingly, for acceptable results at T31 resolution using hybrid coordinates it seems necessary to retain T63 resolution in the computation or else truncation errors become unacceptably large. On the other hand, a case can be made that comparable or better accuracy can be achieved in p coordinates at T42 resolution (compare Fig. 28 with Fig. 26).

Finally, Fig. 29 shows the heating rates at 700 mb for cases 7 and 8 versus case 1. Because vertical interpolation uses the time-averaged coordinate in both cases 7 and 8, whereas this is not so for case 1, the latter is considered to be most realistic. The top panel shows the effect of time averaging on model versus p coordinates, and the bottom panel shows the effects of weighting with Δp as in Eq. (23). In both cases the contour interval is 0.1 K/day and maximum differences are about 0.5 K/day. Some effects of the topography, and thus the coordinate system, are present in the bottom panel, but all differences shown here, and at all other levels, are quite small compared with those in the previous figures.

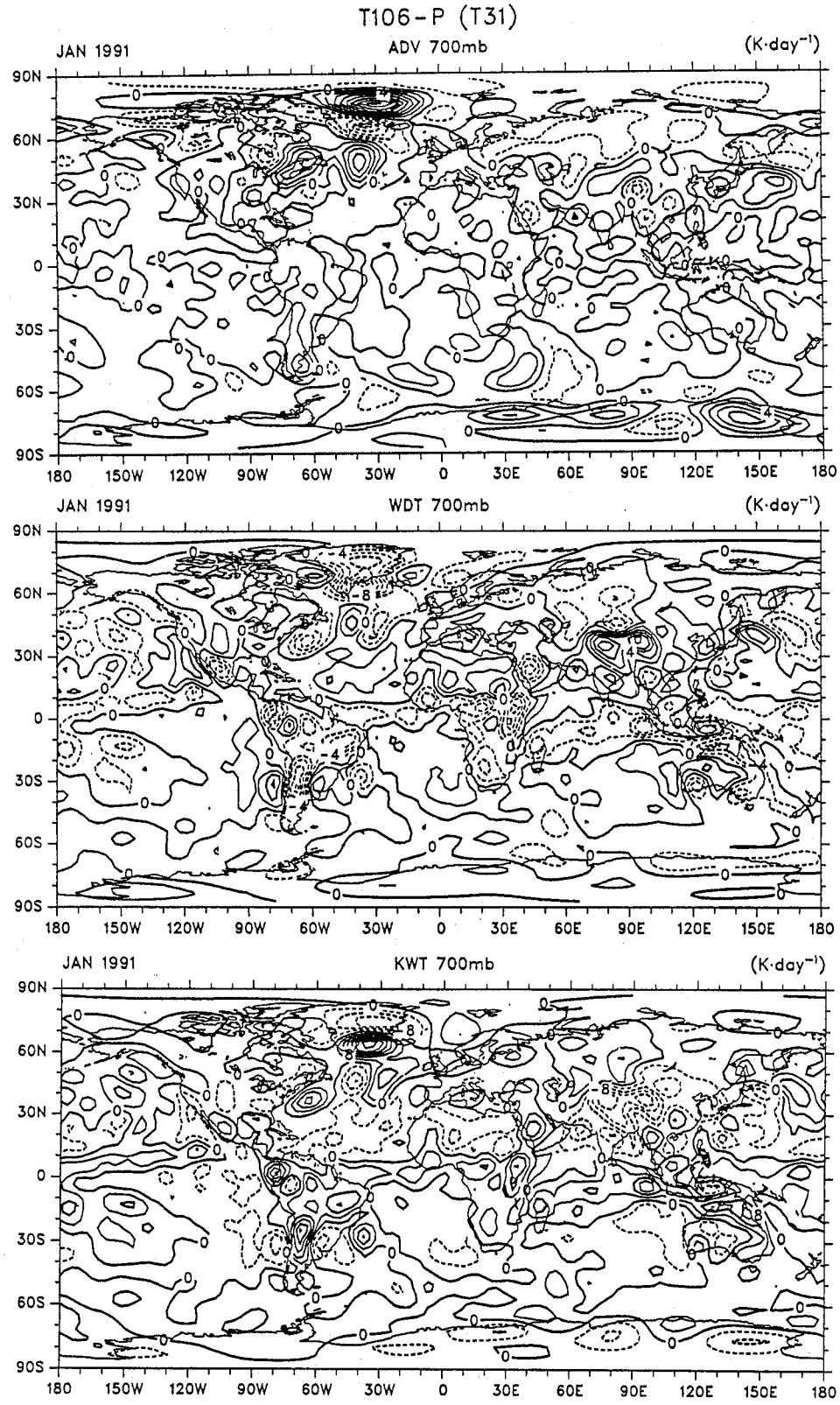

Fig. 21. For January 1991 at 0000 UTC the terms ADV, WDT, and KWT at 700 mb from the full calculation at T106 resolution in p coordinates with results truncated at T31. Units are K/day and the contour interval is 2, 2, and 4 K/day respectively. The negative values are dashed.

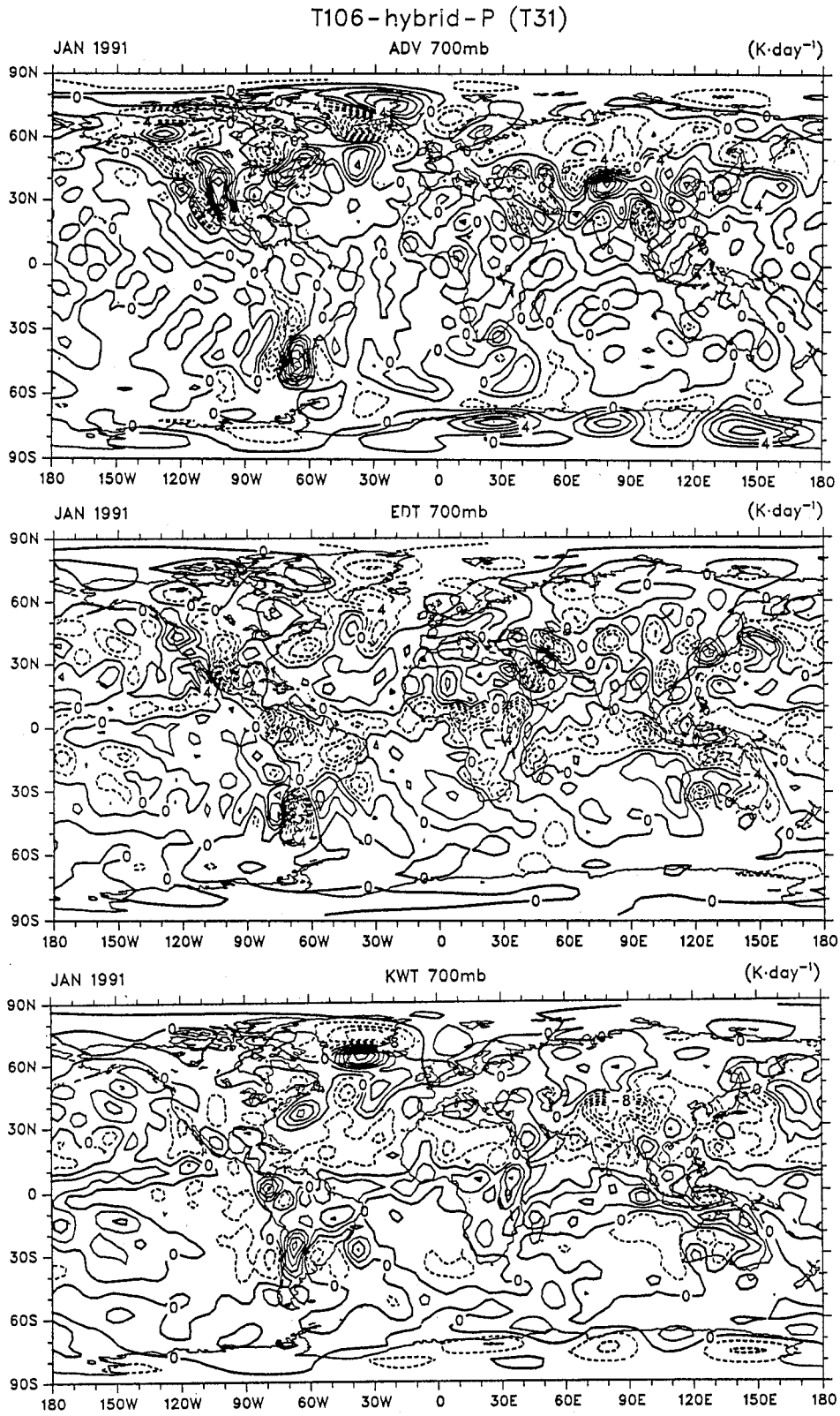

Fig. 22. For January 1991 at 0000 UTC the terms ADV, EDT, and KWT at 700 mb from the full calculation at T106 resolution in hybrid coordinates with results interpolated to p, time averaged, and then truncated at T31. Units are K/day and the contour interval is 2, 2, and 4 K/day respectively. The negative values are dashed.

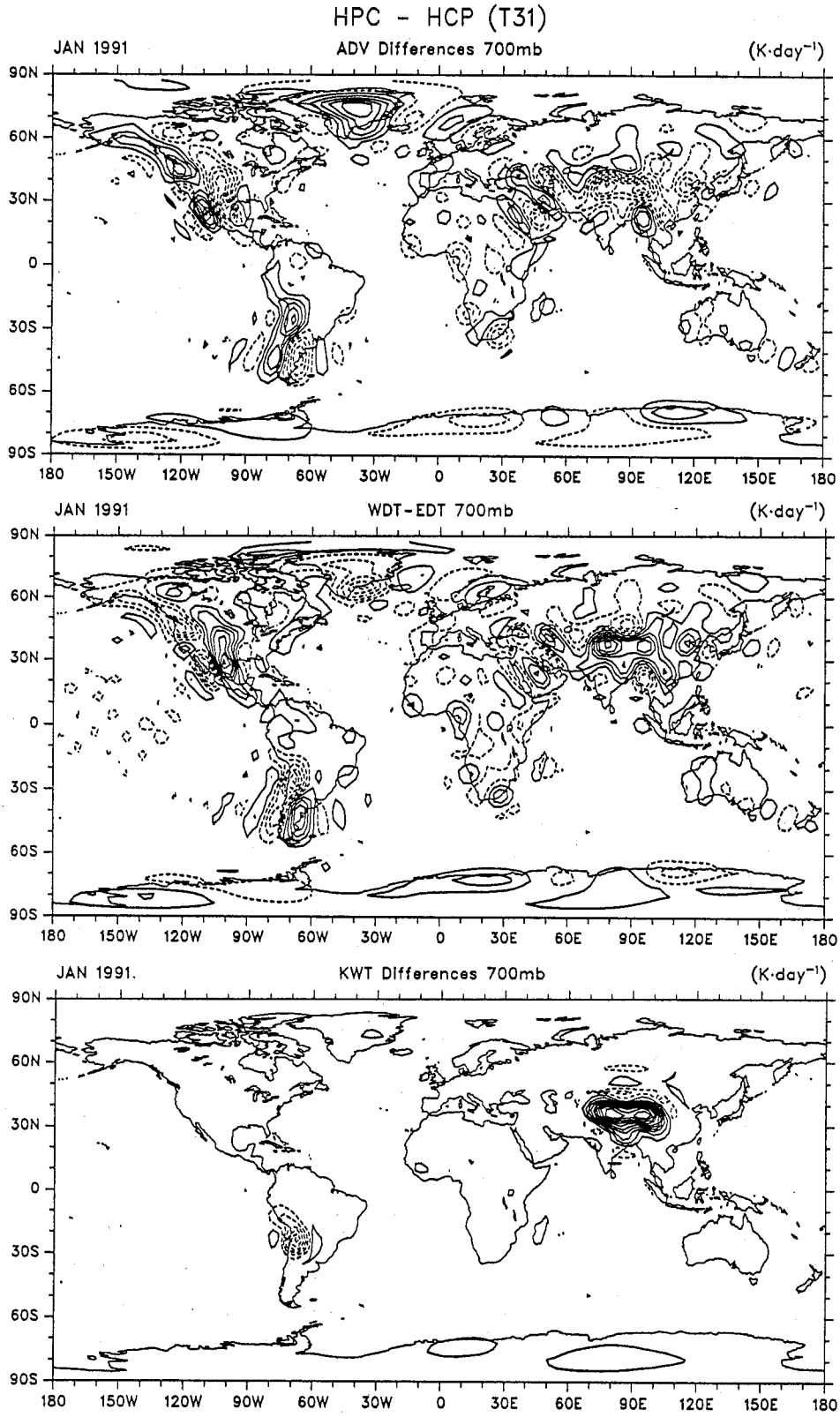

Fig. 23. Differences between the terms in Figs. 21 and 22. Units are K/day and the contour interval is 2, 2, and 0.25 K/day respectively. The first contour is $\pm 1, \pm 1$ *and* ± 0.125 *with negative values dashed.*

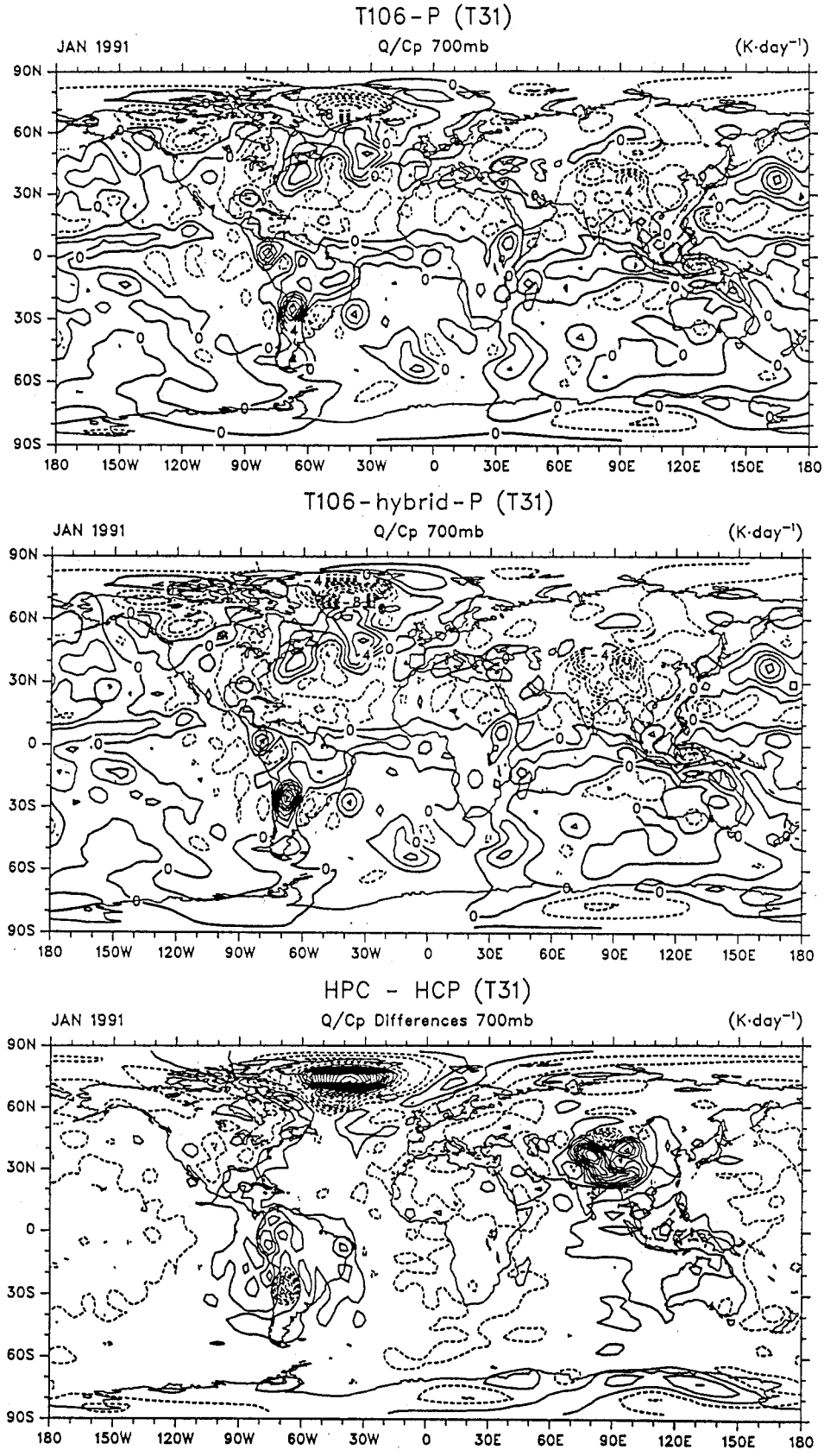

Fig. 24. For January 1991 at 0000 UTC Q/c_p at 700 mb from p coordinates (Fig. 21) (top), hybrid coordinates (Fig. 22) (middle) and their difference (bottom) truncated at T31. Units are K/day and the contour interval is 2, 2, and 0.5 K/day respectively. The first contour is ± 0.25 for the latter and negative values are dashed.

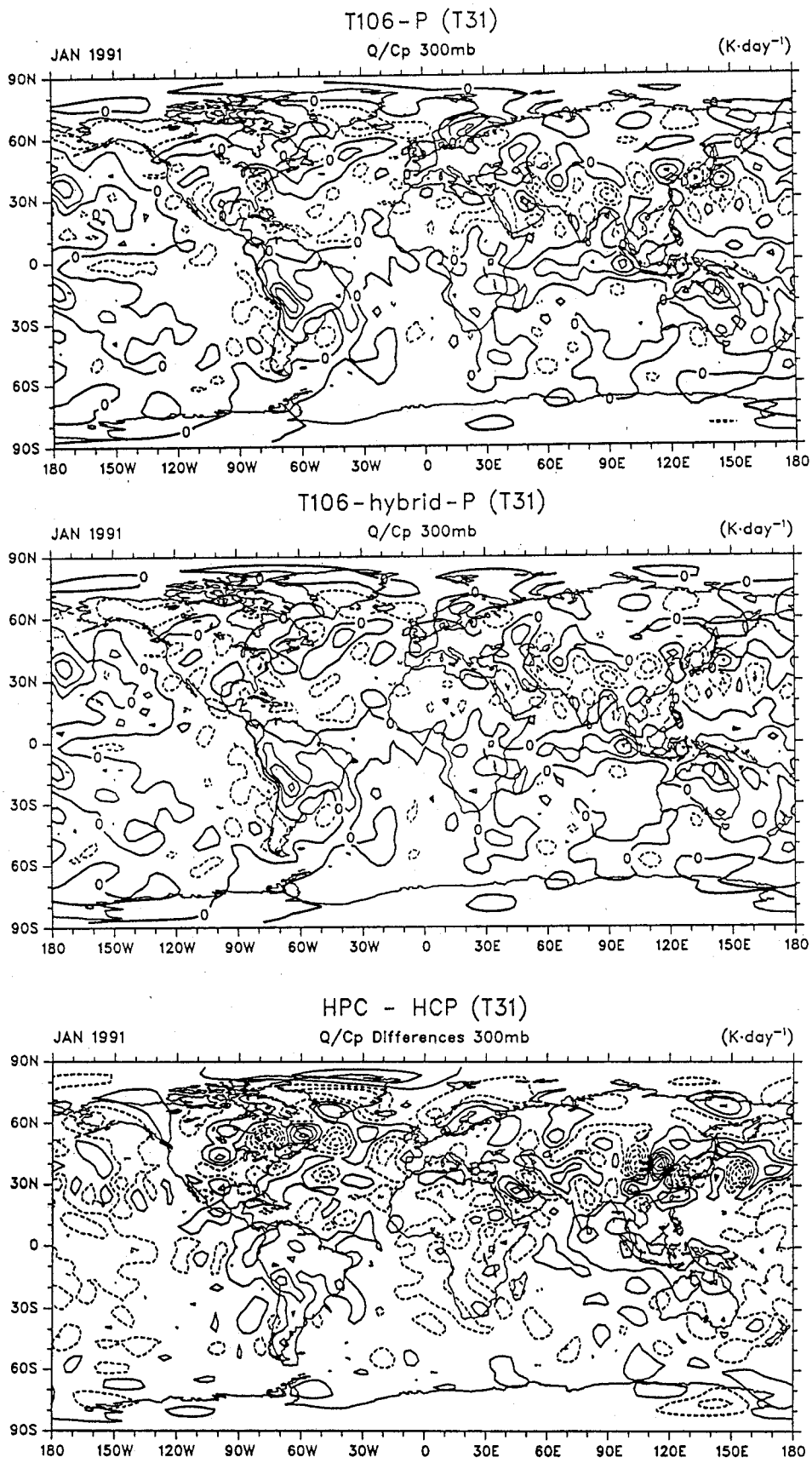

Fig. 25. As in Fig. 24 but for 300 mb. Q/c_p with the contour interval is 2, 2, and 0.5 K/day respectively. The first contour is ± 0.25 for the latter and negative values are dashed.

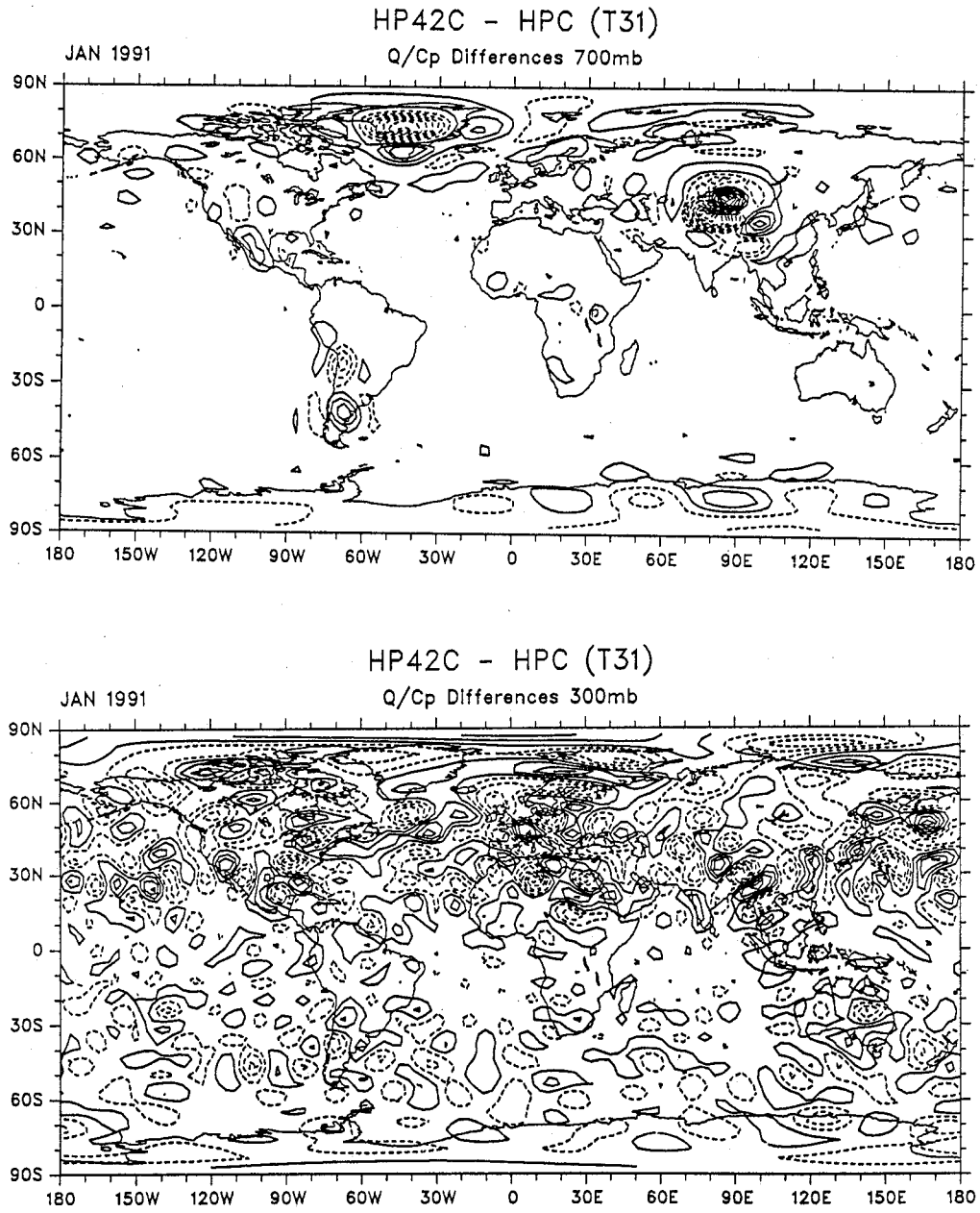

Fig. 26. Effects of truncation in p coordinates to T42 resolution before performing the heat budget. Shown at T31 resolution is the difference difference from the top panel in Fig. 24 at 700 mb (top) and the difference from the top panel of Fig. 25 at 300 mb (lower). The contour interval is 0.5 and 0.1 K/day respectively. The first contour is ± 0.25 *and* ± 0.05 *with negative values dashed.*

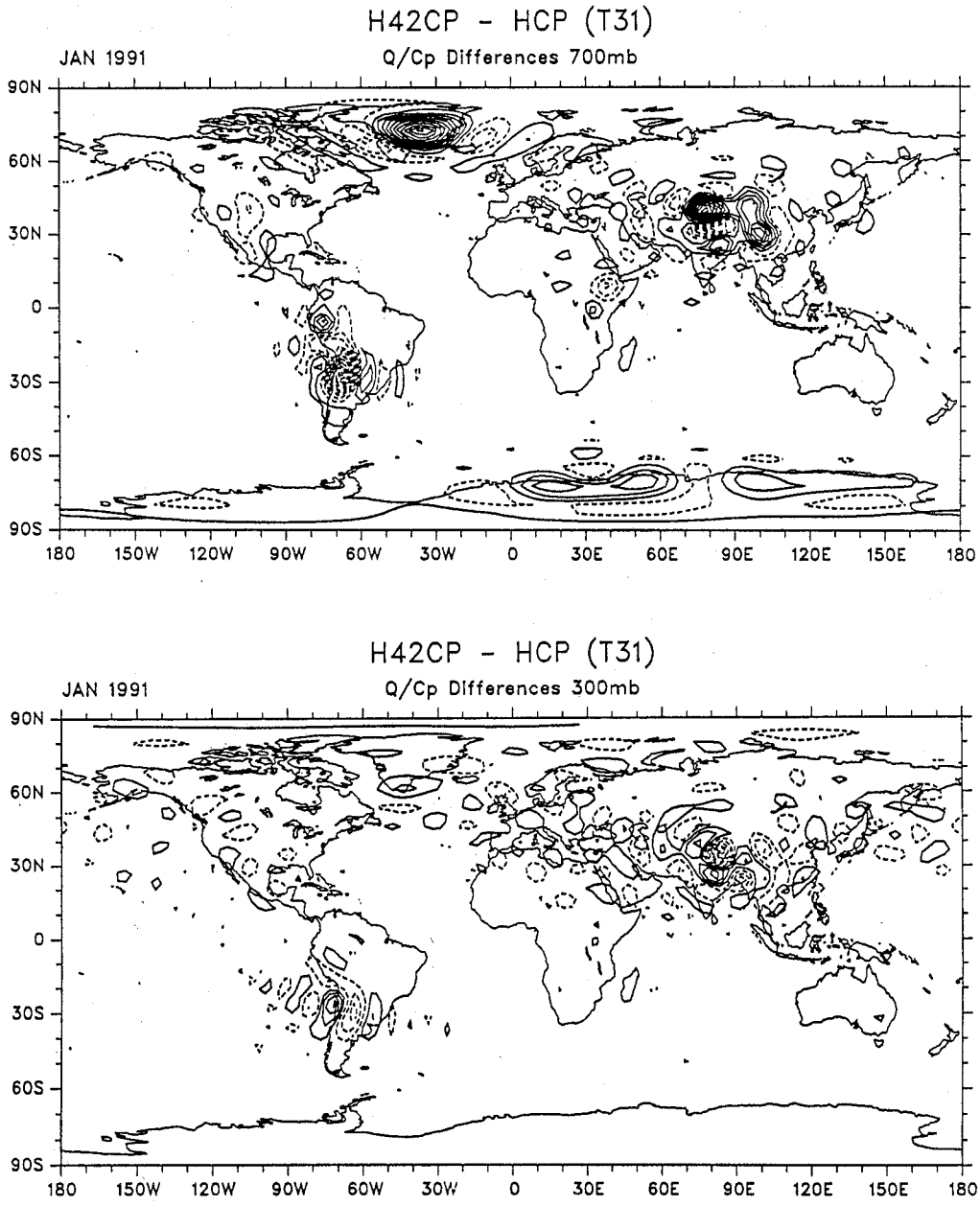

Fig. 27. Effects of truncation in hybrid coordinates to T42 resolution before performing the heat budget. Shown at T31 resolution is the difference difference from the middle panel in Fig. 24 at 700 mb (top) and the difference from the middle panel of Fig. 25 at 300 mb (lower). The contour interval is 1.0 and 0.5 K/day respectively. The first contour is ± 0.5 *and* ± 0.25 *with negative values dashed.*

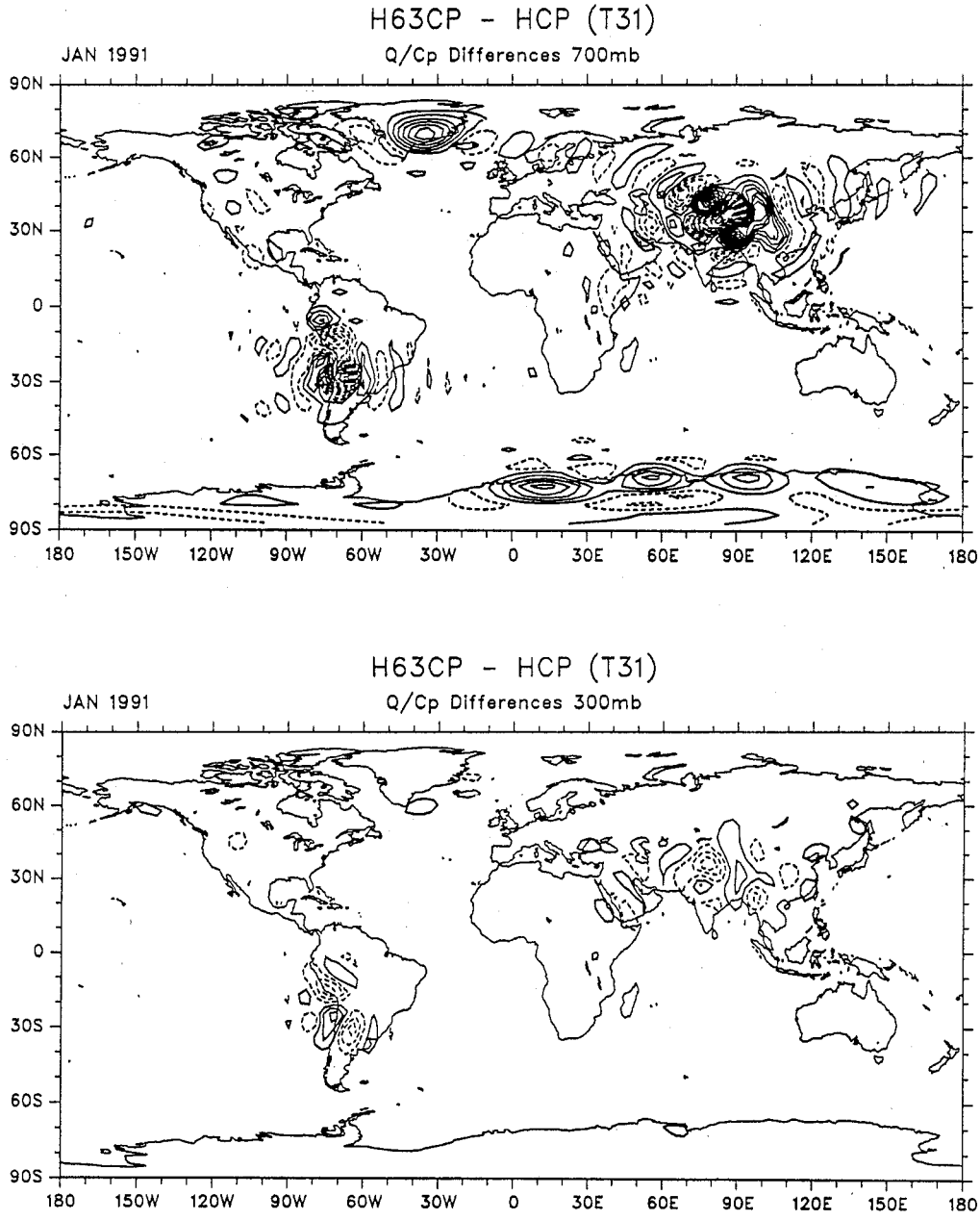

Fig. 28. Effects of truncation in hybrid coordinates to T63 resolution before performing the heat budget. Shown at T31 resolution is the difference difference from the middle panel in Fig. 24 at 700 mb (top) and the difference from the middle panel of Fig. 25 at 300 mb (lower). The contour interval is 0.5 and 0.25 K/day respectively. The first contour is ±0.25 and ±0.125 with negative values dashed.

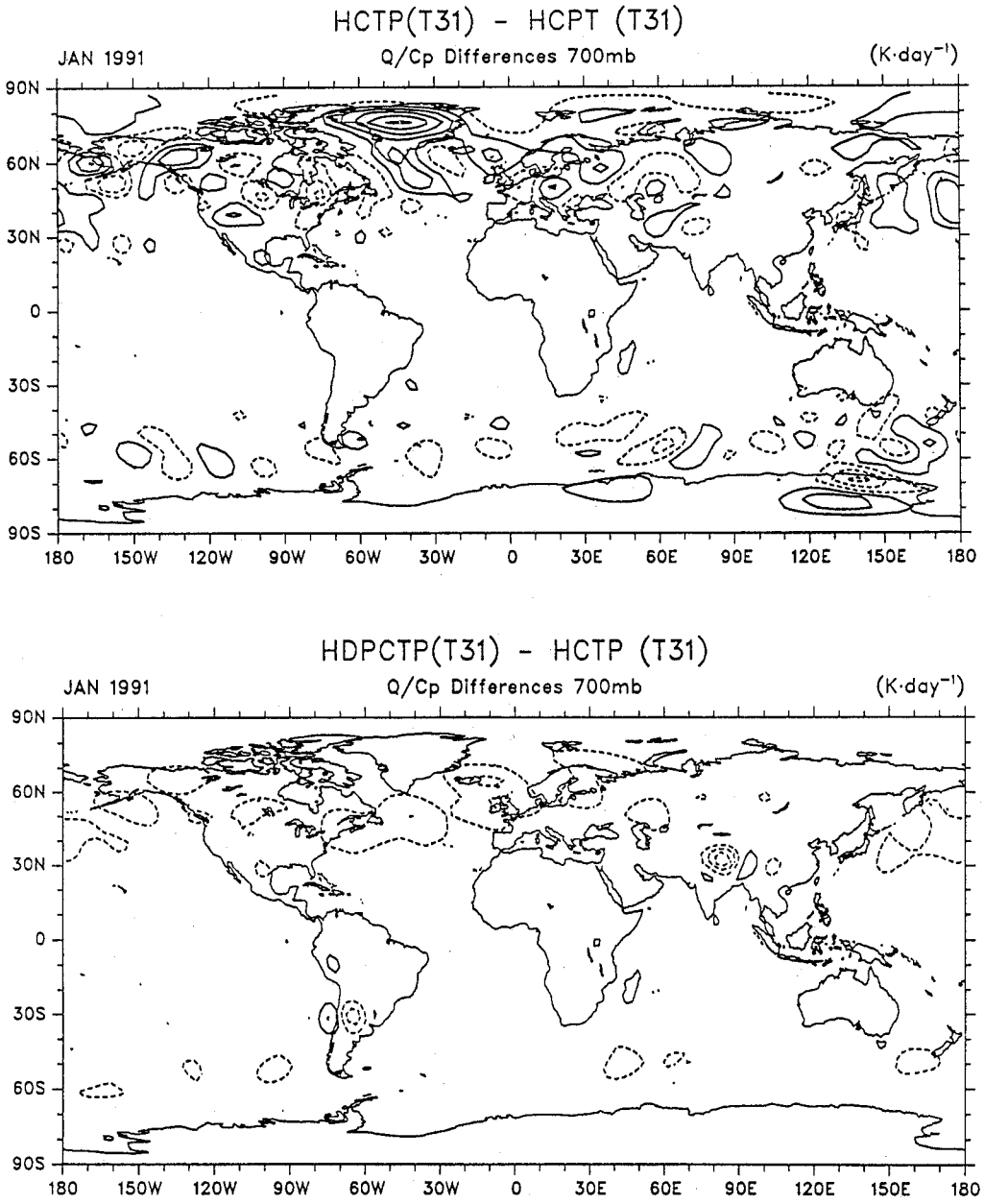

Fig. 29. Effects on Q/c_p at 700 mb of time averaging in hybrid coordinates. Shown at T31 resolution is the difference from the middle panel in Fig. 24 (i.e., full resolution hybrid coordinate calculation, but time-averaged in η before interpolation to p minus time-averaged after interpolation to p) (top) and the additional difference when Δp weighting is included (see Eq. 23) (bottom). The contour interval is 0.1 K/day and the first contour is ± 0.05 with negative values dashed.

7. Conclusions

Hoerling and Sanford (1993) have previously evaluated estimates of atmospheric heating using residual techniques, as we have here, and they compared use of model (in this case sigma) and pressure coordinates. They do not say how they handled the time averaging. They used the older algorithms for interpolating all fields to p and showed results only for vertical integrals and zonal means, both of which are greatly impacted by how the below ground part is handled and the lower bound of integration for the vertical integral, and how the results are interpolated to p-levels for the zonal means. Moreover, they only show fields truncated at wave 10, so that influences of mountains are spread throughout the globe. Such influences are clearly seen coming out from Greenland and the Himalayan complex, especially at lower vertical resolution integrations using p coordinates. Their results show the benefit of using a high (50 mb) vertical resolution for these calculations.

We have documented algorithms from ECMWF which have been implemented in the CCM modular processor for deriving below-ground pressure-level data from model-level (hybrid or sigma) data. The effects are also documented and they are found to reduce unrealistic features below ground, and thus facilitate comparisons of model with analyzed data. A new sea level pressure reduction algorithm has been tested and shown to greatly improve previous problems below high mountains.

New datasets are becoming available on the model levels, minimizing any loss of information for subsequent analysis and diagnosis of the atmosphere. However, the volumes of data are a major obstacle so that changes in resolution prove desirable. As we have noted, changes in resolution are not well posed mathematically in model coordinates because the coordinate system itself also changes. We have shown that very large errors can arise in a thermodynamic equation budget for one month if the model data are truncated to T42 resolution for producing results at T31 resolution, but that truncation to T63 resolution produces more acceptable errors. No matter what method is used, errors arise from interpolation to p surfaces. However, there seems to be a lot to recommend continued use of the traditional representation on constant pressure surfaces provided sufficient vertical resolution is retained. Here we used a 50 mb vertical resolution. The main disadvantage is the potential contamination of regions outside of the below-ground areas when fields are used in calcula-

tions such as application of the divergence operator. In addition, vertical integrals are more readily peformed in model coordinates.

We have also noted that the meaning of a time average in different coordinates is not the same and it is not always possible to relate the time average in p to that in η, but in practical terms, the differences are quite small and probably negligible for most purposes.

Another outstanding problem with data on model levels is the fact that the model surface often does not correspond with the earth's real surface. Nevertheless, overall the advantages in working in the model coordinate system are the ability to handle the lower boundary properly although changes in resolution somewhat compromise accuracies, especially on small scales.

References

ECMWF (1990) Research Manual 2, Appendix 6. ECMWF Meteorological Bulletin.

Fortelius, C., and E. Holopainen, 1990: Comparison of energy source estimates derived from atmospheric circulation data with satellite measurements of net radiation. *J. Climate*, **3**, 646–660.

Hack, J. J., B. A. Boville, B. P. Briegleb, J. T. Kiehl, P. J. Rasch and D. L. Williamson, 1993: Description of the NCAR Community Climate Model (CCM2). NCAR Tech Note NCAR/TN-382+STR. 108 pp.

Hoerling, M. P., and L. L. Sanford, 1993: On the uncertainty in estimates of atmospheric heating due to data postprocessing. *J. Climate*, **6**, 168-174.

Mesinger, F., and R. E. Treadon, 1993: "Horizontal" reduction of pressure to sea level: Comparison against the NMC's "Shuell" method. *Mon. Wea. Rev.*, (submitted).

O'Brien, J. J., 1970: Alternative solutions to the classical vertical velocity problem. *J. Appl. Meteor.*, **9**, 197–203.

Haseler, J., and G. Sakellarides, 1986: Description of the ECMWF model post processing system. ECMWF Tech. Memorandum No. 121., 63 pp plus appendix.

Shen, R., E. R. Reiter and J. F. Bresch, 1986: Vertical interpolation of meteorological variables. *Mon. Wea. Rev.*, **114**, 123–134.

Simmons, A. J., and D. M. Burridge, 1981: An energy and angular-momentum conserving vertical finite-difference scheme and hybrid vertical coordinates. *Mon. Wea. Rev.*, **109**, 758–766.

Simmons, A. J., and R. Strüfing, 1983: Numerical forecasts of stratospheric warming events using a model with a hybrid vertical coordinate. *Quart. J. Roy. Meteor. Soc.*, **109**, 81–111.

Trenberth, K. E., 1991a: Climate diagnostics from global analyses: Conservation of mass in ECMWF analyses. *J. Climate*, **4**, 707-722.

Trenberth, K. E., 1991b: Storm tracks in the southern hemisphere. *J. Atmos. Sci.*, **48**, 2159–2178.

Trenberth, K. E., 1992: Global Analyses from ECMWF and Atlas of 1000 to 10 mb Circulation Statistics. NCAR Tech. Note. NCAR/TN–373+STR, 191 pp plus 24 fiche .

Trenberth, K. E., and J. G. Olson, 1988: An evaluation and intercomparison of global analyses from NMC and ECMWF. *Bull. Amer. Meteor. Soc.*, **69**, 1047–1057.

Trenberth, K. E., and A. Solomon, 1993: Implications of global atmospheric spatial spectra for processing and displaying data. *J. Climate*, **6**, 531–545.